cmgh
CELLULAR AND MOLECULAR GASTROENTEROLOGY AND HEPATOLOGY

ORIGINAL RESEARCH

Over-expressed Phospholamban in Cancer-associated Fibroblasts Is a Driver for CMS4 Subtype Colorectal Cancer Formation

Tao Li,[1,2,7,*] Yuxiang Fei,[2,3,7,*] Xu Sun,[4,5,*] Jun Zhu,[4,5] Xin Fang,[2] Fanjun Meng,[2] Danyi Wang,[2] Xu Zhang,[6] Chao Liu,[2,3,7] and Qianming Du[1,2,7]

[1]General Clinical Research Center, Nanjing First Hospital, Nanjing Medical University, Nanjing, P.R. China; [2]School of Basic Medicine and Clinical Pharmacy, China Pharmaceutical University, Nanjing, P.R. China; [3]Department of Pharmacy, Nanjing First Hospital, Nanjing Medical University, Nanjing, P.R. China; [4]Department of Pharmacy, Nanjing Luhe People's Hospital, Nanjing, China; [5]Department of Pharmacy, Nanjing Luhe People's Hospital, Yangzhou University, Nanjing, P.R. China; [6]Department of Pharmacy, Chengdu Integrated TCM & Western Medicine Hospital, Chengdu University of TCM, Chengdu, P. R. China; and [7]Nanjing First Hospital, Nanjing University of Chinese Medicine, Nanjing, P.R. China

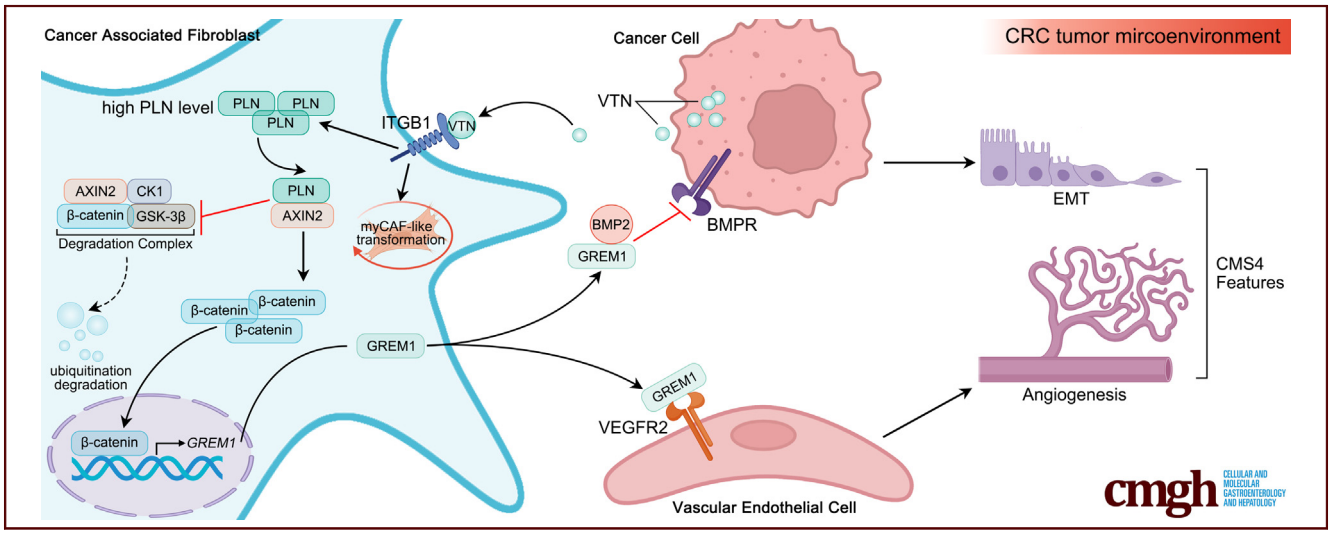

SUMMARY

Over-expressed phospholamban in cancer-associated fibroblasts of colorectal cancer is a driver for CMS4 subtype formation via inducing epithelial mesenchymal transition and angiogenesis. Mechanistically, phospholamban strongly upregulates β-catenin activity, which leads gremlin 1-BMP2/gremlin 1-VEGFR2 intercellular signals activation in the microenvironment.

BACKGROUND & AIMS: Heterogeneity is the malignancy feature of colorectal cancer (CRC), which augments the difficulty of CRC treatment. Consensus molecular subtypes (CMSs) classified CRC into 4 subtypes. CMS4 is the most aggressive subtype, characterized with epithelial mesenchymal transition (EMT) and angiogenesis activation. However, the mechanism of CMS4 formation still remains unclear. We aimed to investigate the role of phospholamban (PLN) on CMS4 formation.

METHODS: Immunohistochemistry and Western blotting were used to detected PLN expressions. Transwell and wound-healing assays were used to evaluate migration and invasion of HCT116 and HT29. Tube formation assay was used to evaluate angiogenesis of HUVECs. GST pull-down was used to detected the interaction between PLN and AXIN2. The CAF-CT26 spleen co-transplantation mouse model was built to evaluate PLN's effects on CRC metastasis.

RESULTS: PLN knockdown reversed CAFs' conditional medium (CM)-induced EMT, cell migration, and angiogenesis ($P < .01$). PLN strongly bound to AXIN2, the main component of β-catenin degradation complex, and PLN knockdown increased β-catenin ubiquitination in CAFs ($P < .01$). PLN knockdown blocked GREM1 secretion ($P < .01$), and PLN overexpression-induced EMT, cell migration, and angiogenesis were blocked by anti-GREM1 neutralizing antibody ($P < .01$). Knockdown of BMP2 and VEGFR2 reversed CAFs' CM induced EMT and angiogenesis effects, respectively ($P < .01$). PLN knockdown attenuated CAFs mediated tumor promoting effects *in vivo* ($P < .01$).

CONCLUSIONS: PLN competitively binds with AXIN2 to increase β-catenin activity in CAFs. β-catenin signal induces GREM1 secretion, driving EMT and angiogenesis via BMP2 and

VEGFR2, respectively. These findings demonstrate that PLN is a driver for CMS4 formation. *(Cell Mol Gastroenterol Hepatol 2025;19:101524; https://doi.org/10.1016/j.jcmgh.2025.101524)*

Keywords: Angiogenesis; Cancer-associated Fibroblasts; Colorectal Cancer; Epithelial Mesenchymal Transition; Phospholamban.

This article has an accompanying editorial.

Colorectal cancer (CRC) is one of the most commonly occurred cancers with a high mortality worldwide.[1] Due to its high heterogeneity, patients with CRC often tend to be vastly different in clinical outcomes and drug responses, which makes elaborate clinical management hard to carry out and common therapeutical approaches difficult to apply to all types of patients with CRC.[2] To overcome such complexity, a consensus molecular subtypes (CMS) classification system was built for CRC in 2015, which divided CRC into 4 subtypes (CMS1–4) with distinguishable features. Among the 4 subtypes, CMS4, the mesenchymal type, is regarded as the most aggressive one with the worst survival rates.[3] Serrated adenocarcinoma, the high-malignancy pathologic type of CRC, commonly belongs to CMS4. The molecular biology features of CMS4 includes upregulation of genes mainly related to epithelial mesenchymal transition (EMT), angiogenesis, and matrix remodeling, which means the CMS4 subtype has the highest metastasis and recurrence rates.[4] Because metastasis and recurrence are the main causes of death from CRC during the advanced stages, understanding CMS4 is critical. Until now, limited research has focused on CMS4, and the mechanisms underlying its formation still remain unclear. Therefore, a better understanding of CMS4 subtype features could power the diagnosis, treatment, and personalized care of patients with CRC.

Phospholamban (PLN) is an endogenous antagonist of sarcoplasmic reticulum Ca^{2+}-ATPase (ATP2A2). PLN is primarily found in cardiac muscle cells, and act as a regulator of heart inotropic response via cAMP-dependent Ca^{2+} pump activation in physiologic condition.[5] The recognized pathologic role of PLN is inducing heart failure by downregulating ATP1A2 activity when PLN is overexpressed.[6] Beyond the cardiovascular system, recent research has found PLN also expresses in neurons and regulates sleep and executive functions, indicating that PLN may potentially have multiple regulation roles.[7] However, whether PLN has a regulation role in cancer carcinogenesis or progression remains uninvestigated until now.

Our data shows that PLN is highly expressed in the CMS4 subtype of CRC tumor tissues and is negatively correlated with the survival rates of patients with CRC. Interestingly, we found PLN exclusively expressed in cancer-associated fibroblasts (CAFs) rather than cancer cells. As an important member of the tumor microenvironment (TME), CAFs are closely associated with poor prognosis in CRC. Numerous evidence has demonstrated that CAFs can drive cancer evolution to adapt the TME via reprograming cancer cells and immune cells in a paracrine way.[8] Based on this background, in this study, we discuss whether CAF-derived PLN was a driver for CMS4 subtype formation, as well as whether PLN signal had any influences on CRC metastasis via paracrine regulation in CRC TME.

Results

PLN is a Marker of Mesenchymal CRC

Given CMS4 is the most aggressive subtype of CRC, we aimed to identify the key regulatory genes driving the CMS4 phenotype formation. Using CMScaller, a CRC consensus molecular subtyping algorithm, we classified CRC patients into 2 cohorts (The Cancer Genome Atlas [TCGA] and Gene Set Enrichment (GSE) 106582) (Figure 1*A*) and identified the significantly upregulated genes in the CMS4 subtype. Eight genes were found upregulated in CMS4 across both cohorts (Figure 1*B–C*). mRNA levels of the 8 upregulated genes (*PLN, SFRP2, MYH11, DES, CNN1, ACTG2, MGP,* and *THBS4*) were then analyzed in CRC clinical samples. *PLN, SFRP2,* and *MYH11* were highly expressed in CRC tumor tissues compared with adjacent normal tissues, with *PLN* showing the most significant upregulation. Notably, PLN expression levels were higher in serrated adenocarcinoma tissues (the pathologic type of CMS4 subtype) than in tubular adenocarcinoma (Figure 1*D–E*). Consistent with mRNA levels, PLN protein levels were also upregulated in CRC tumor tissues, with serrated adenocarcinoma exhibiting higher expression than tubular adenocarcinoma, conforming PLN was a marker gene of the CMS4 subtype, the mesenchymal CRC. In addition, patients with CMS4 subtype CRC with high PLN expression levels in tumor tissues had lower survival rates when compared with those with low PLN expression (Figure 1*F–I*). We further detected PLN expressions in a clinical CRC tissue microarray, analyzed its relation with patients' survival and metastasis, and found that high PLN expressed group had

***Authors share co-first authorship.**

Abbreviations used in this paper: **ANOVA, analysis of variance; BMP, bone morphogenetic protein; CAF, cancer-associated fibroblast; CM, conditional medium; CMS, consensus molecular subtype; Co-IP, co-immunoprecipitation; CRC, colorectal cancer; DMEM, Dulbecco's Modified Eagle Medium; DVL, dishevelled; ELISA, enzyme-linked immunosorbent assay; EMT, epithelial mesenchymal transition; FBS, fetal bovine serum; GAPDH, glyceraldehyde-3-phosphate dehydrogenase; GO, Gene Ontology; GSE, Gene Set Enrichment; HUVEC, human umbilical vein endothelial cell; ITGB1, integrin subunit beta 1; KEGG, Kyoto Encyclopedia of Genes and Genomes; mCRC, metastatic colorectal cancer; myCAF, myofibroblastic cancer-associated fibroblast; NF, normal fibroblast; PBS, phosphate-buffered saline; PLN, phospholamban; prCRC, primary colorectal cancer; PVDF, polyvinylidene fluoride; qPCR, quantitative polymerase chain reaction; rBMP, recombinant BMP2; rGREM1, recombinant GREM1 protein; SBM, SERCA binding motif; scRNA-seq, single-cell RNA sequencing; SD, standard deviation; shRNA, short hairpin RNA; TCGA, The Cancer Genome Atlas; TEG, tegatrabetan; TME, tumor microenvironment; VEGFR2, VEGF receptor-2; VIM, vimentin; VTN, vitronectin.**

Most current article

2352-345X
https://doi.org/10.1016/j.jcmgh.2025.101524

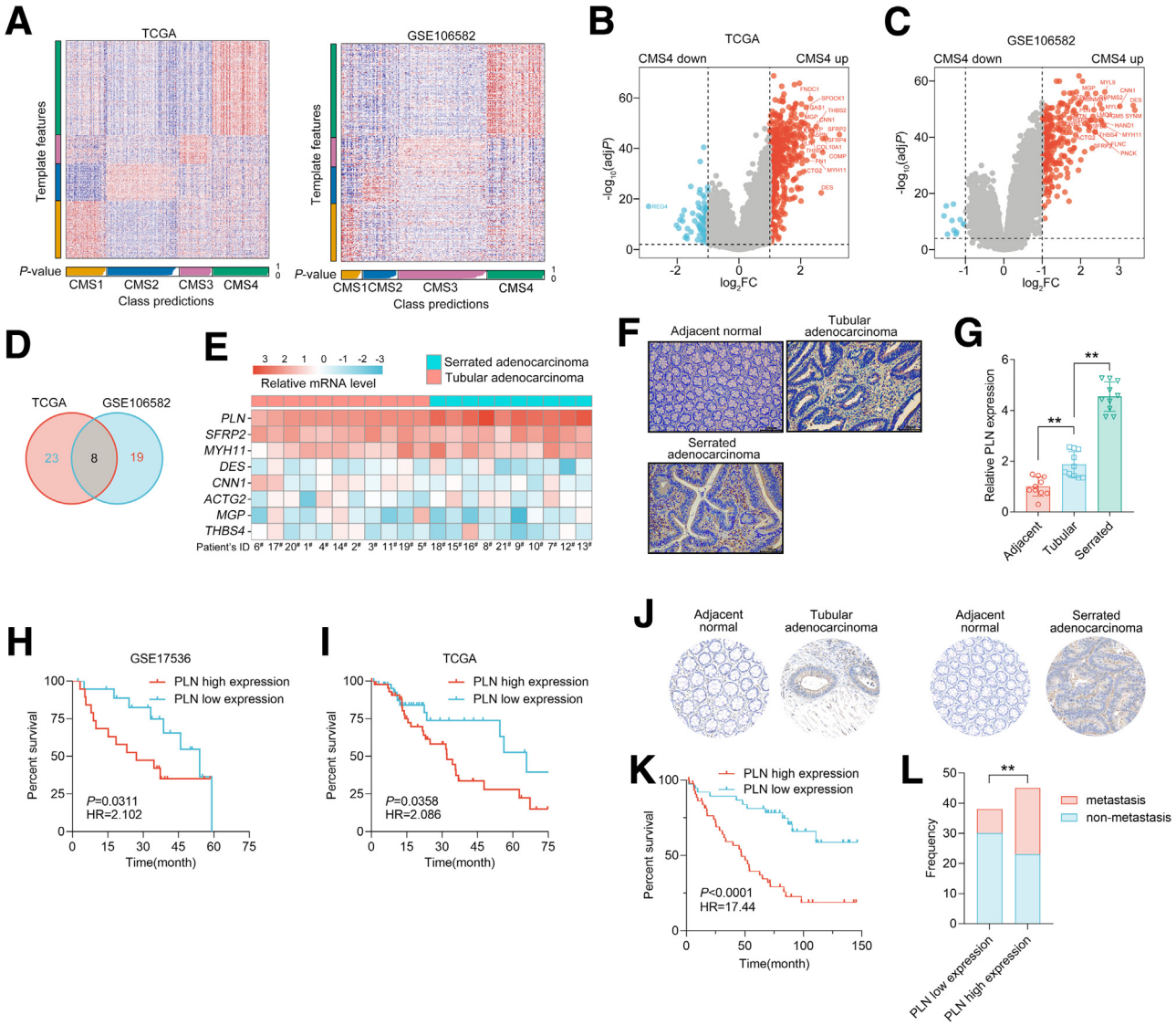

Figure 1. (*A*) Heatmap of CMS classification for TCGA-COAD and GSE 106582 datasets. (*B*) Differently expressed genes (-$\log_{10}$(adj*P*)>2, |log2FC|>1) in CMS4 subtype tumor tissues of TCGA-COAD dataset. (*C*) differently expressed genes (-$\log_{10}$(adj*P*)>2, |log2FC|>1) in CMS4 subtype tumor tissues of GSE106582 dataset. (*D*) Venn plot for intersection of up-regulated genes in TCGA and GSE106582 datasets (*PLN, SFRP2, MYH11, DES, CNN1, ACTG2, MGP,* and *THBS4*). (*E*) mRNA levels of *PLN, SFRP2, MYH11, DES, CNN1, ACTG2, MGP,* and *THBS4* in patients with CRC-originated tumor tissues were detected by qPCR. (*F–G*) PLN expression in patients with CRC-originated tumor and adjacent normal tissues were detected by IHC. (*H–I*) Kaplan-Meier curves for overall survival analysis of patients with CMS4 subtype CRC from GSE17536 and TCGA-COAD datasets. (*J–L*) representative images of anti-PLN IHC staining, Kaplan-Meier curve of overall survival analysis, and frequency of PLN high or low expression samples in patients with metastatic and non-metastatic CRC from a tissue array. All experiments have been repeated at least 3 times independently. $^{**}P < .01$.

lower survival rates and more metastasis, indicating PLN levels were closely related with clinical outcomes of CRC (Figure 1*J–L*). Taken together, these findings suggest that PLN may be a potential driver of CMS4 subtype formation and tumor progression.

PLN is Preferentially Expressed in CAFs of CRC Lesions

To identify the primary cell type expressing PLN in CRC tumor tissues, we analyzed single-cell RNA sequencing (scRNA-seq) data, which revealed that PLN was predominantly expressed in fibroblasts (Figure 2*A*). In CRC clinical samples, the colocation rates of PLN^+ and FAP^+ (a fibroblast marker) were significantly higher than PLN^+ and $EpCAM^+$ (a tumor cell marker); in line with clinical samples, PLN protein levels in CAFs isolated from CRC tissues were significantly higher than human CRC cell lines (HCT116, LOVO, HT29, SW480) and normal fibroblasts (NFs), confirming that PLN was preferentially expressed in CAFs of CRC lesions (Figure 2*B–D*). As gene function enrichment analysis shown in Figure 2*E–G* illustrates, high PLN

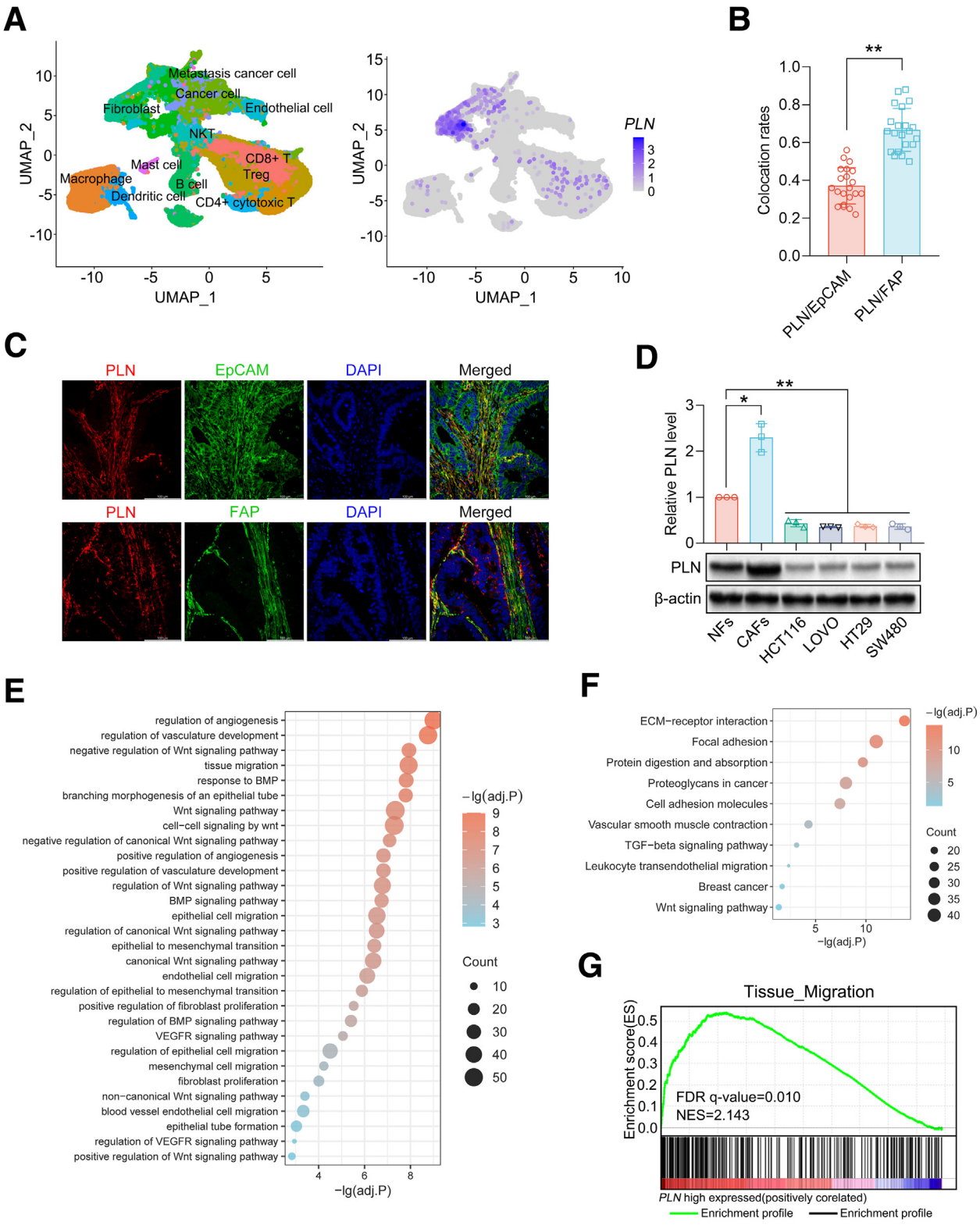

Figure 2. (*A*) *Left panel*: UMAP plot of cell type distribution for scRNAseq data from CRC tumor tissues (GSE225857, GSE231559, GSE178318, and GSE221575); *right panel*: UMAP plot of PLN expression distribution in the single cell RNAseq data. (*B–C*) quantification and representative photos for PLN/EpCAM and PLN/FAP colocation in patients with CRC-originated tumor tissues were measured by IHC. (*D*) PLN expressions in NFs and CAFs, as well as CRC cell lines (HCT116, LOVO, HT29, and SW480), were detected by Western blotting. (*E–G*) GO, KEGG, and Gene Set Enrichment Analysis (GSEA) for up-regulated genes of PLN^{high} vs. PLN^{low} in CRC tissues from TCGA-COAD dataset. All experiments have been repeated at least 3 times independently. $^{*}P < .05$; $^{**}P < .01$.

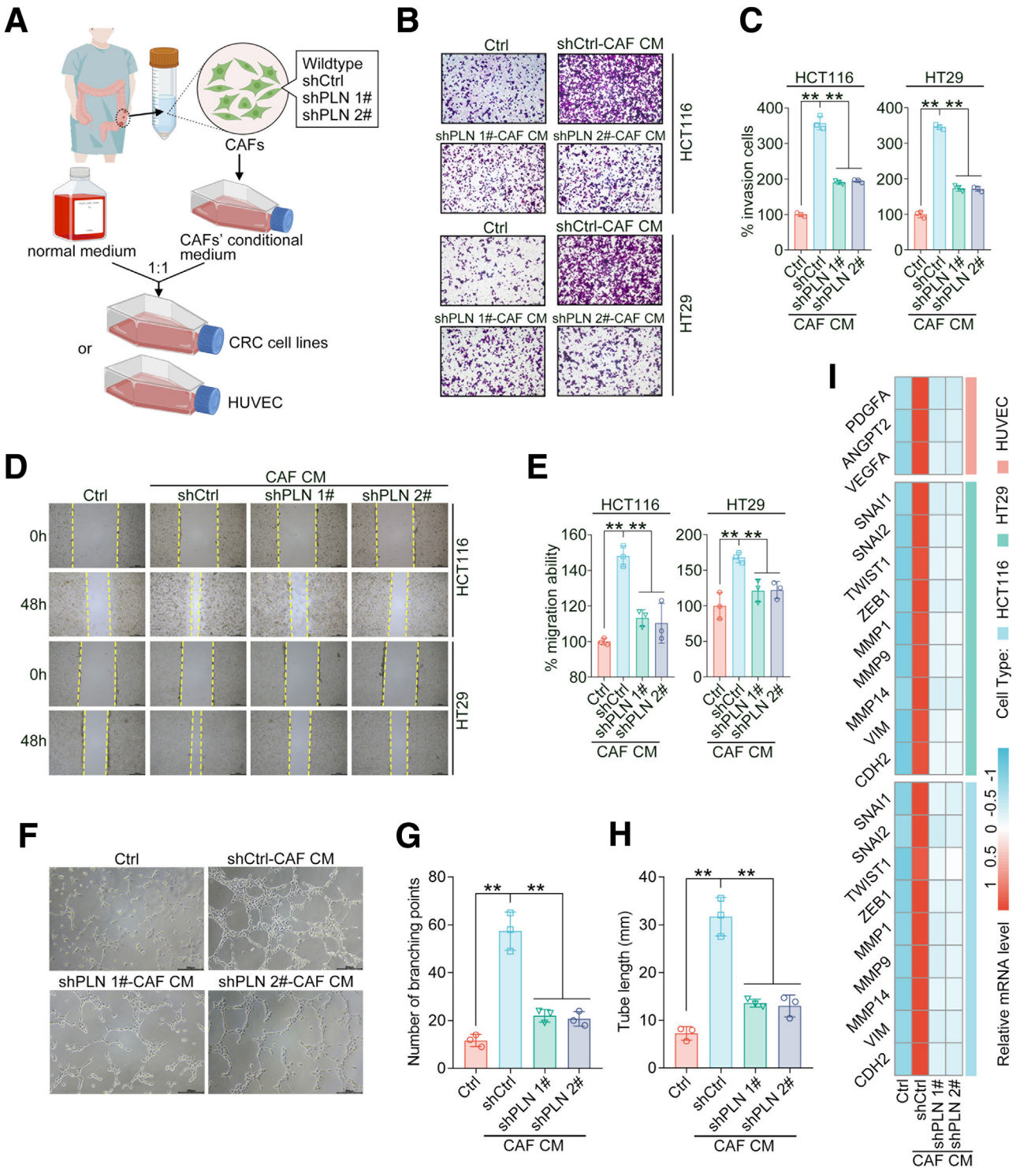

Figure 3. (*A*) Schematic diagram of CAF CM-incubated CRC cell lines and HUVEC cells. (*B–C*) representative photos and quantification of Transwell assay in HCT116 and HT29 cells after incubated with/without CAF CMs for 48 hours. (*D–E*) Representative photos and quantification of wound-healing assay in HCT116 and HT29 cells after incubation with/without CAF CMs for 48 hours. (*F–H*) representative photos and quantification of tube formation assay in HUVEC cells after incubation with/without CAF CMs for 48 hours. (*I*) qPCR assay for EMT-related genes in HCT116 and HT29 and angiogenesis-related genes in HUVEC cells. All experiments have been repeated at least 3 times independently. $^{**}P < .01$.

expression was related with EMT, cell migration, angiogenesis, and fibroblast proliferation, as well as the Wnt, BMP, and VEGFR signaling pathways. These biological processes and signaling events were closely linked to the CMS4-like phenotype, suggesting that PLN may play a pivotal role in formation of the CMS4 subtype.

PLN Knockdown Impaired CAFs-induced Cancer Cell Migration and Angiogenesis

Given that PLN was preferentially expressed in CAFs and possibly related to CMS4 subtype formation, we investigated the influences of CAF-derived PLN on phenotype transformation of CRC cell lines and human umbilical vein endothelial cells (HUVECs) (Figure 3*A*). Conditional medium (CM) from CRC patient-derived CAFs significantly enhanced the invasion and migration capabilities of HCT116 and HT29 cells, whereas PLN knockdown in CAFs reversed such migration-inducing effects (Figure 3*B*–*E*). Similarly, CAF-derived CM also strongly induced HUVEC mesh formation, which was significantly reduced upon PLN knockdown in CAFs (Figure 3*F*–*H*). In addition, CAF-derived CM induced EMT and angiogenesis-related gene upregulation in CRC cell lines (HCT116, HT29) and HUVEC, respectively (Figure 3*I*). Consistent with these findings in human-derived models, CM from mouse-derived CAFs also enhanced invasion and EMT-related genes upregulation in CT26 (a mouse CRC cell line) (Figure 4*A*–*C*), as well as prompted mesh formation and upregulated angiogenesis-related genes in C166 (a mouse vascular endothelial cell line) (Figure 4*D*–*G*). Notably, these effects were reversed by PLN knockdown in CAFs.

Collectively, this evidence demonstrates that CAF-derived PLN is a critical inducer for cell phenotype transformation, driving EMT in cancer cells and angiogenesis in vascular endothelial cells. Given that EMT and angiogenesis are the key features of CMS4 subtype of CRC, indicating that PLN is an important driver for CMS4 subtype formation.

PLN Maintained High Wnt/β-catenin Signaling Activity in CAFs

As evidence in Result 2 showed that PLN was closely related to Wnt signaling, we investigated whether PLN had any regulatory roles in this pathway. Previous evidence indicated β-catenin level in CAFs were significantly upregulated, leading to the activation of Wnt signaling.[9] Therefore, we investigated whether PLN could upregulate β-catenin level. First, we analyzed the similarity of amino acid sequences between PLN and β-catenin, as well as between ATP2A2 (a known binding partner of PLN) and AXIN2 (a component of β-catenin degradation complex).[10] As presented in Figure 5*A*, ATP2A2 and AXIN2 had 2 similarity regions, and PLN and β-catenin had 1 similarity in their amino acid sequences. Additionally, the molecular docking analysis revealed a high docking score between PLN and AXIN2 (Figure 5*B*), indicating that PLN had a high possibility to bind with AXIN2.

The binding between PLN and AXIN2 in both human and mouse CAFs was further verified by co-immunoprecipitation (CoIP) assay (Figure 5*C*), indicating that PLN might be involved in β-catenin degradation. Given that research had shown that phosphorylation of PLN can disrupt its binding to ATP2A2,[11,12] we further investigated the impact of PLN phosphorylation on its interaction with AXIN2. Interestingly, we found that mutation of PLN phosphorylation sites (Ser16 or Thr17) had no significant influences on the interaction between PLN and AXIN2, as well as CAF CM-mediated invasion-promoting effects in both HCT116 and HT29 cells (Figure 5*D*–*G*). Quantitative polymerase chain reaction (qPCR) results demonstrated that PLN knockdown had no influences on β-catenin (encodes by *CTNNB1*) mRNA levels but significantly reduced its protein levels in CAFs (Figure 5*H*–*K*). Based on this evidence, we hypothesized that PLN competitively binds to AXIN2, which disorganizes the β-catenin degradation complex formation and increases cellular levels of β-catenin, thereby activating Wnt/β-catenin signaling. CoIP results further supported this hypothesis, showing that PLN knockdown in both human and mouse CAFs enhanced the binding between β-catenin and AXIN2, CK1, and GSK-3β (components of β-catenin degradation complex), whereas PLN overexpression impaired these interactions (Figure 5*L*–*M*). Because PLN has been reported to bind ATP2A2 via its SERCA binding motif (SBM),[13] we generated SBM-deleted PLN fusion protein (His-PLN-Mut) to verify whether PLN also binds AXIN2 through SBM (Figure 6*A*). GST pull-down results showed that PLN directly interacted with AXIN2, whereas deletion of SBM disrupted this binding, indicating that SBM was essential for PLN's interaction with AXIN2 (Figure 6*B*–*C*). Furthermore, we observed that PLN impaired the binding between β-catenin and AXIN2, and this effect was abolished when the SBM was deleted (Figure 6*D*–*E*).

Next, we checked whether PLN could influence protein degradation of β-catenin in CAFs. We found that β-catenin ubiquitylation levels increased and protein levels decreased following PLN knockdown in both human and mouse CAFs (Figure 6*F*–*K*). Furthermore, the downregulation of β-catenin induced by PLN knockdown in CAFs was blocked by proteasome inhibitor MG132, whereas PLN overexpression in NFs upregulated β-catenin levels, which was also blocked by MG132 (Figure 6*L*–*O*). To directly observed the influence of PLN on β-catenin degradation complex formation, we examined the colocalization of β-catenin and AXIN2. The results revealed that PLN knockdown in CAFs (both human- and mouse-sourced) enhanced colocation of β-catenin and AXIN2, whereas PLN overexpression in NFs (both human- and mouse-sourced) reduced the colocation (Figure 6*P*; Figure 7*A*–*E*). These results indicated that PLN regulated β-catenin levels in a proteasome-dependent manner. Additionally, we detected the mRNA levels of Wnt/β-catenin signaling downstream target genes and found that PLN knockdown in CAFs significantly downregulated the majority of these genes, whereas PLN overexpression in NFs significantly upregulated these genes (Figure 7*F*). Taken together, evidence in this section demonstrated that PLN could disrupt the formation of β-catenin degradation complex, resulting in elevated β-catenin levels and activity in CAFs.

PLN-induced GREM1 Secretion-mediated EMT and Angiogenesis in CRC

Following the elevated targeted genes of Wnt/β-catenin signaling being identified in Figure 7*F*, with *GREM1*

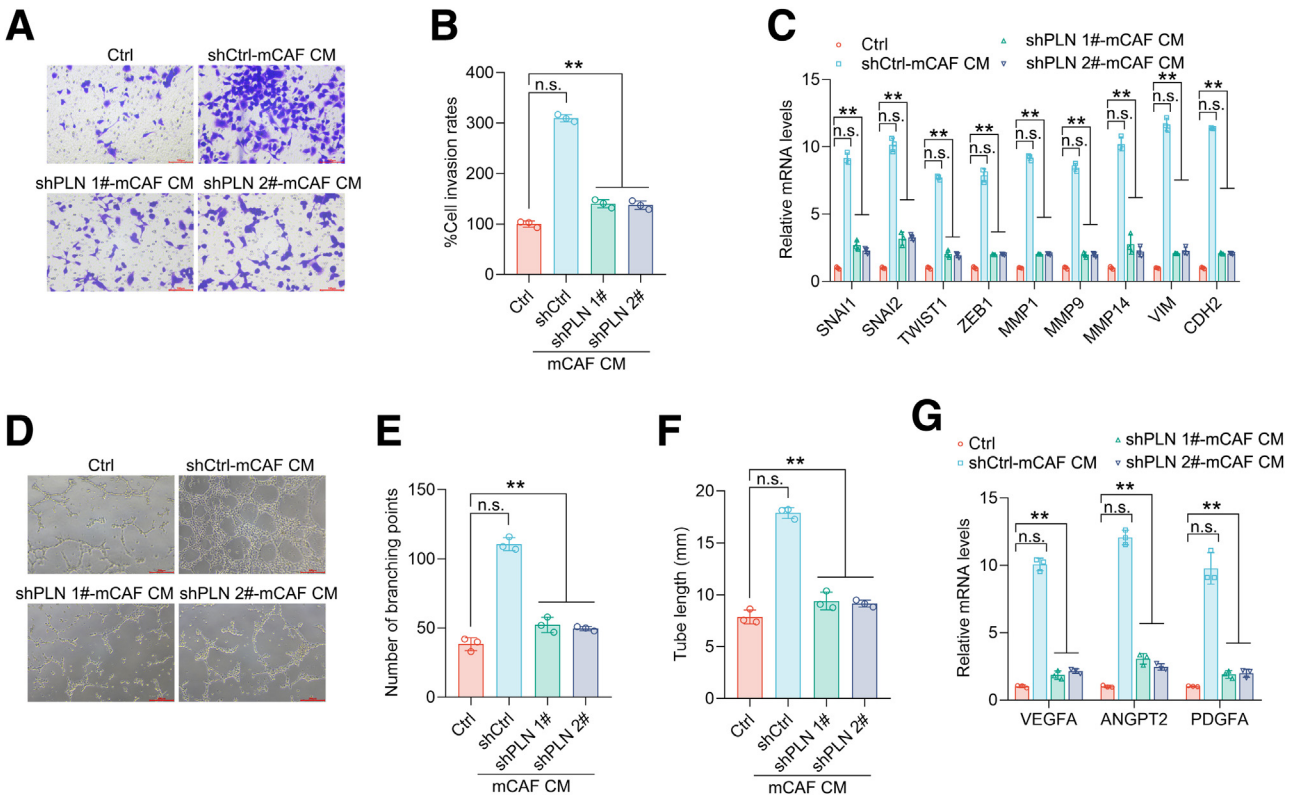

Figure 4. (*A–B*) representative images of Transwell assay (*A*) and quantification of cell invasion rates (*B*) in CT26 incubated with CM from mouse CAFs (mCAF) transfected with shCtrl, shPLN 1# or shPLN 2# for 48 hours. (*C*) qPCR analysis of EMT marker genes mRNA levels in CT26 treated as described in (*A–B*). (*D–G*) representative images of tube formation assay (*D*), quantification of branching points (*E*), tube length (*F*), and qPCR analysis of angiogenesis marker genes mRNA levels (*G*) in C166 cells (mouse vascular endothelial cell line) treated as described in (*A–B*). n.s., no significant differences; $^{**}P < .01$.

exhibiting the most significant changes, we also found in scRNA-seq data of CRC that *GREM1* was distinctly expressed in CAFs, and mRNA levels of *PLN* and *GREM1* in CRC tumor tissues had a strong correlation (Figure 7*G–H*); In addition, we assessed the levels of secretary protein (PLAUR, MMP7, NRCAM, CD44, VEGFA, FGF18, EDN1, GREM1) encoded by these elevated targeted genes of Wnt/β-catenin signaling, and found that GREM1 was consistently present at high levels and was significantly reduced upon PLN knockdown in both human and mouse CAFs, whereas levels of the other proteins retained no significant changes (Figure 7*I–P*). Furthermore, overexpression of PLN increased *GREM1* mRNA levels in NFs, which was significantly reversed by the β-catenin selective inhibitor, tegatrabetan (TEG) (Figure 7*Q*); in addition, overexpression of PLN increased GREM1 secretion in NFs, whereas mutation of PLN phosphorylation sites (Ser16 or Thr17) had no significant influence on this effect (Figure 7*R*). These findings suggest that GREM1 is the key gene upregulated by PLN in CAFs.

Next, we checked whether PLN-led EMT and angiogenesis effects in CRC was mediated by GREM1. Firstly, we found that recombinant GREM1 protein (rGREM1) induced HCT116 and HT29 cells invasion and migration in a dose-dependent manner (Figure 7*S–U*; Figure 8*A–C*). rGREM1 also upregulated EMT marker genes expression both in HCT116 and HT29 cells in a dose-dependent manner (Figure 8*D*). In the other aspect, rGREM1 dose-dependently induced mesh formation and angiogenesis-related gene upregulation in HUVEC cells (Figure 8*E–H*). rGREM1-derived invasion and angiogenesis-promoting effects were also observed in mouse CRC cancer cells and vascular cell (CT26 and C166) (Figure 8*I–M*). These findings confirmed that GREM1 was a strong inducer of EMT and angiogenesis in CRC cells. We next tried to verify whether PLN-mediated EMT and angiogenesis effects on CRC cells was dependent on GREM1 secretion. PLN-overexpressed NFs CM significantly induced cell invasion and migration both in HCT116 and HT29 cells, and such effects were blocked by anti-GREM1 neutralizing antibody (Figure 8*N–S*). PLN-overexpressed NFs CM also upregulated EMT marker genes expression, which was expectedly reversed by anti-GREM1 neutralizing antibody (Figure 8*T*). In line with EMT induced by PLN in CRC cells, PLN-overexpressed NFs CM strongly induced mesh formation and angiogenesis-related gene upregulation in HUVEC cells, which were blocked by anti-GREM1 neutralizing antibody (Figure 8*U–W*; Figure 9*A*). The anti-GREM1 neutralizing antibody also effectively blocked invasion and angiogenesis-

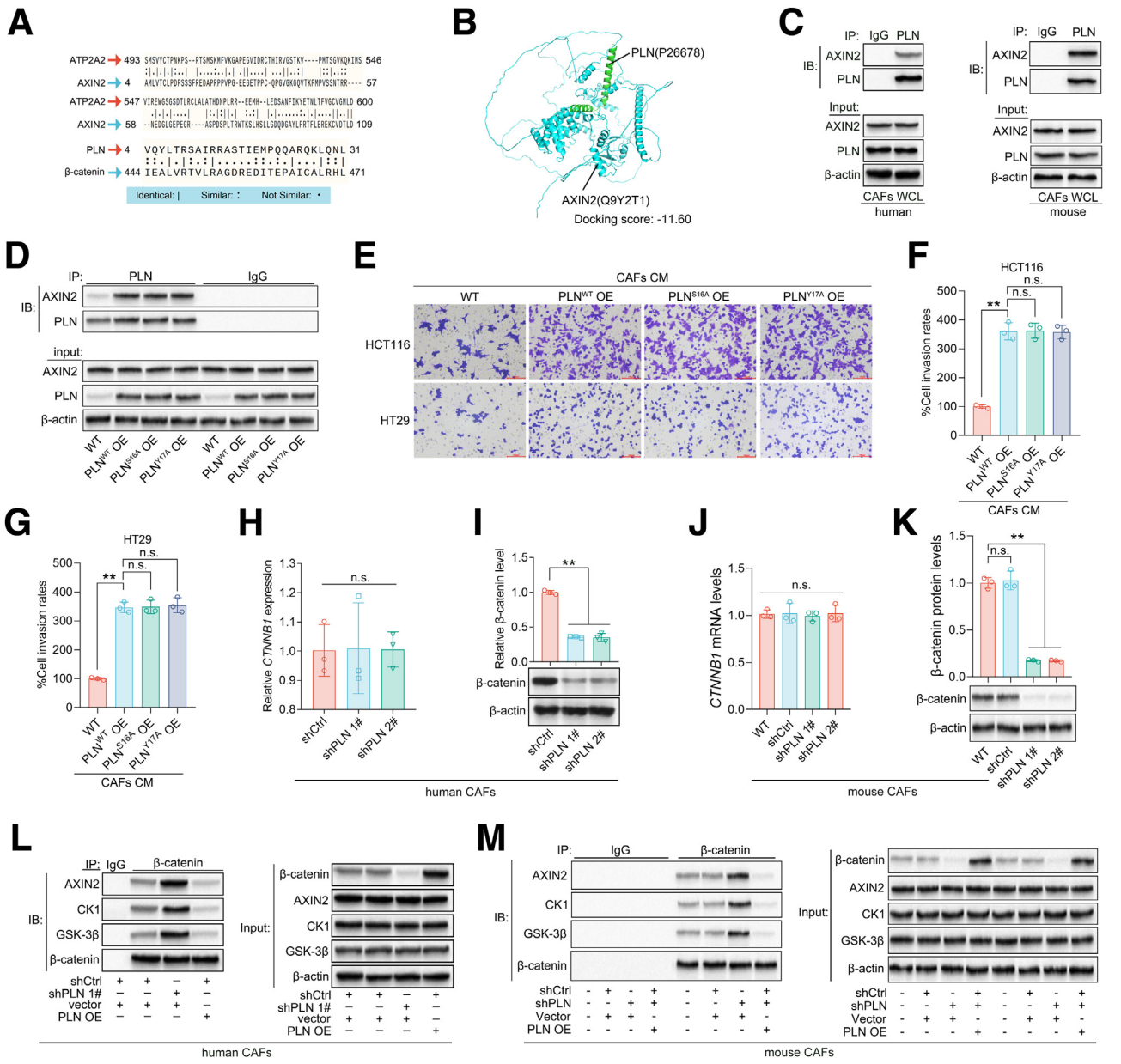

Figure 5. (*A*) Schematic diagram of amino acid sequences alignment analysis. (*B*) Schematic diagram of molecular docking between PLN and AXIN2. (*C*) CoIP analysis of AXIN2 and PLN in human and mouse CAFs' whole cell lysis (WCL). (*D*) CoIP assay of AXIN2 and PLN in human CAFs with wild-type (WT), PLN overexpression (OE), S16A mutated PLN OE, or Y17A mutated PLN OE. (*F–G*) Representative images and cell invasion rates of HCT116 and HT29 cells after incubation with CM from WT PLN OE, S16A mutated PLN OE or Y17A mutated PLN OE CAFs for 48 hours. (*H–K*) qRCR assay of *CTNNB1*, and Western blotting assay of β-catenin in both human and mouse CAFs (shCtrl, or shPLN 1/2# transfected). (*L–M*) CoIP analysis of AXIN2, CK1, GSK-3β, and β-catenin in both human and mouse CAFs (vector, transfected with empty plasmid; PLN OE, transfected with PLN expression plasmid). All experiments have been repeated at least 3 times independently. $^{**}P < .01$; n.s., no significant differences.

promoting effects mediated by PLN-overexpressed NFs CM in mouse models (Figure 9*B–F*). To make the above findings more convincing, we carried out a NFs-CRC cell lines or HUVEC co-culture system based on transwell plates to further investigate the effects of CAF-derived PLN on cell invasion and angiogenesis (Figure 9*G*). The results showed that co-culturing NFs with CRC cells or HUVEC had no significant influences on either cell invasion or angiogenesis, whereas PLN OE in NFs strongly induced both cell invasion and angiogenesis, which were reversed by anti-GREM1 neutralizing antibody (Figure 9*H–O*; Figure 10*A*). In summary, these findings demonstrated that PLN sustained high β-catenin activity in CAFs, leading to induction of GREM1 secretion; and GREM1 functioned as a strong inducer of

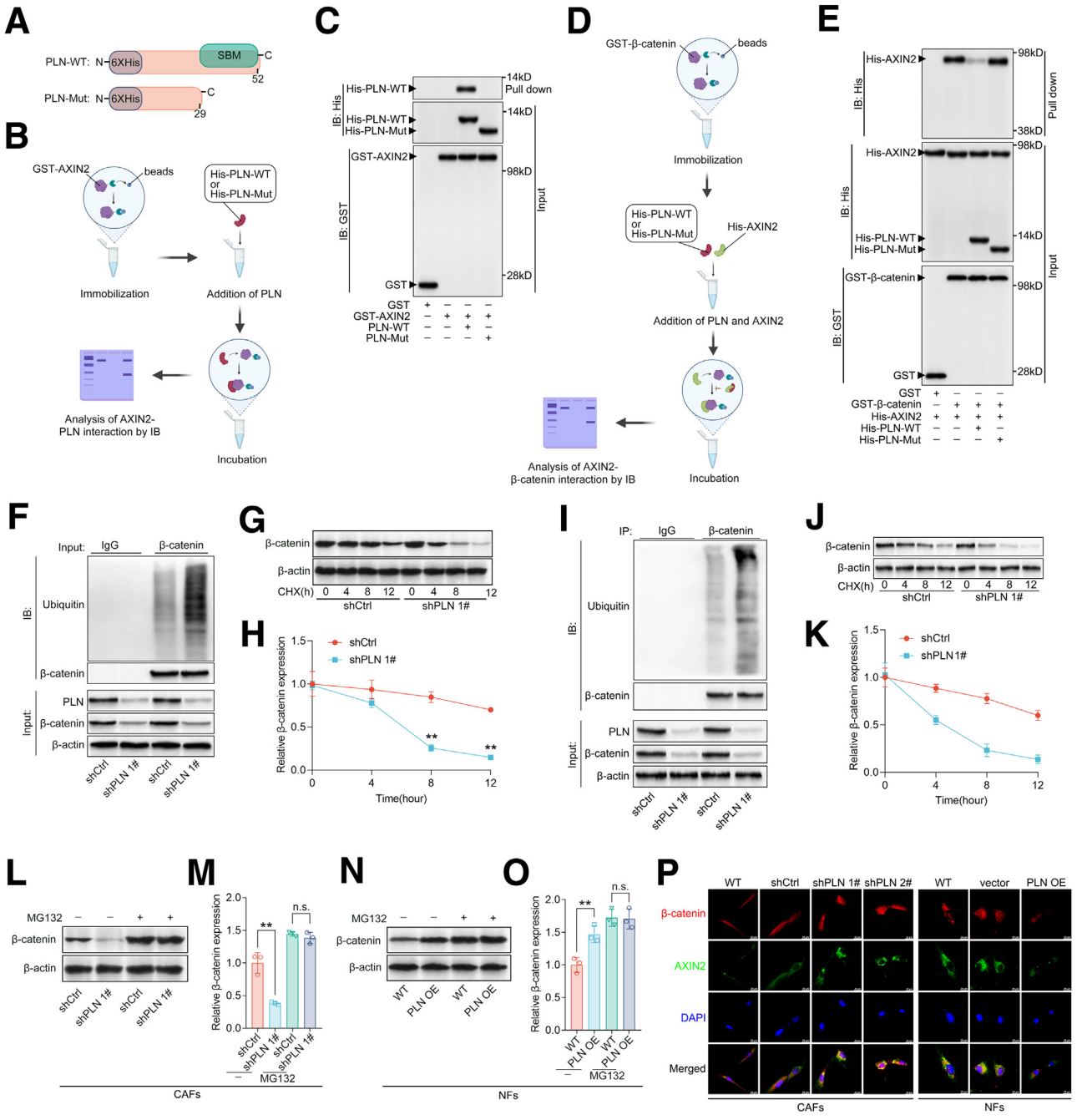

Figure 6. (*A–B*) Schematic diagram of PLN recombinant protein (WT, wildtype; Mut, mutation) and GST pull-down experiment design for AXIN2 and PLN interaction. (*C*) GST-pulldown assay of GST-AXIN2 and His-PLN. (*D*) Schematic diagram of GST pull-down experiment design for influence of PLN on AXIN2 and β-catenin interaction. (*E*) GST pull-down assay of GST-β-catenin, His-AXIN2, and His-PLN. (*F*) Co-IP assay for β-catenin ubiquitylation analysis in human CAFs after incubating with MG132 (10 μmol/L) for 12 hours. (*G–H*) Western blotting bands (*G*) and quantification (*H*) for β-catenin detection in human CAFs after incubating with cycloheximide (CHX, 100 μg/mL) at indicated time points. (*I*) Co-IP assay for β-catenin ubiquitylation analysis in mouse CAFs after incubating with MG132 (10 μmol/L) for 12 hours. (*J–K*) Western blotting bands (*J*) and quantification (*K*) for β-catenin detection in human CAFs after incubating with cycloheximide (CHX, 100 μg/mL) as indicated time points. (*L–O*) Western blotting for β-catenin detection in human CAFs or NFs after incubating with MG132 (10 μmol/L) for 12 hours. (*P*) Representative images of immunofluorescence assay for β-catenin and AXIN2 in human CAFs transfected with shCtrl, shPLN-1#, or in PLN-2#, or NFs transfected with empty vector or PLN OE. All experiments have been repeated at least 3 times independently. $^{**}P < .01$; n.s., no significant differences.

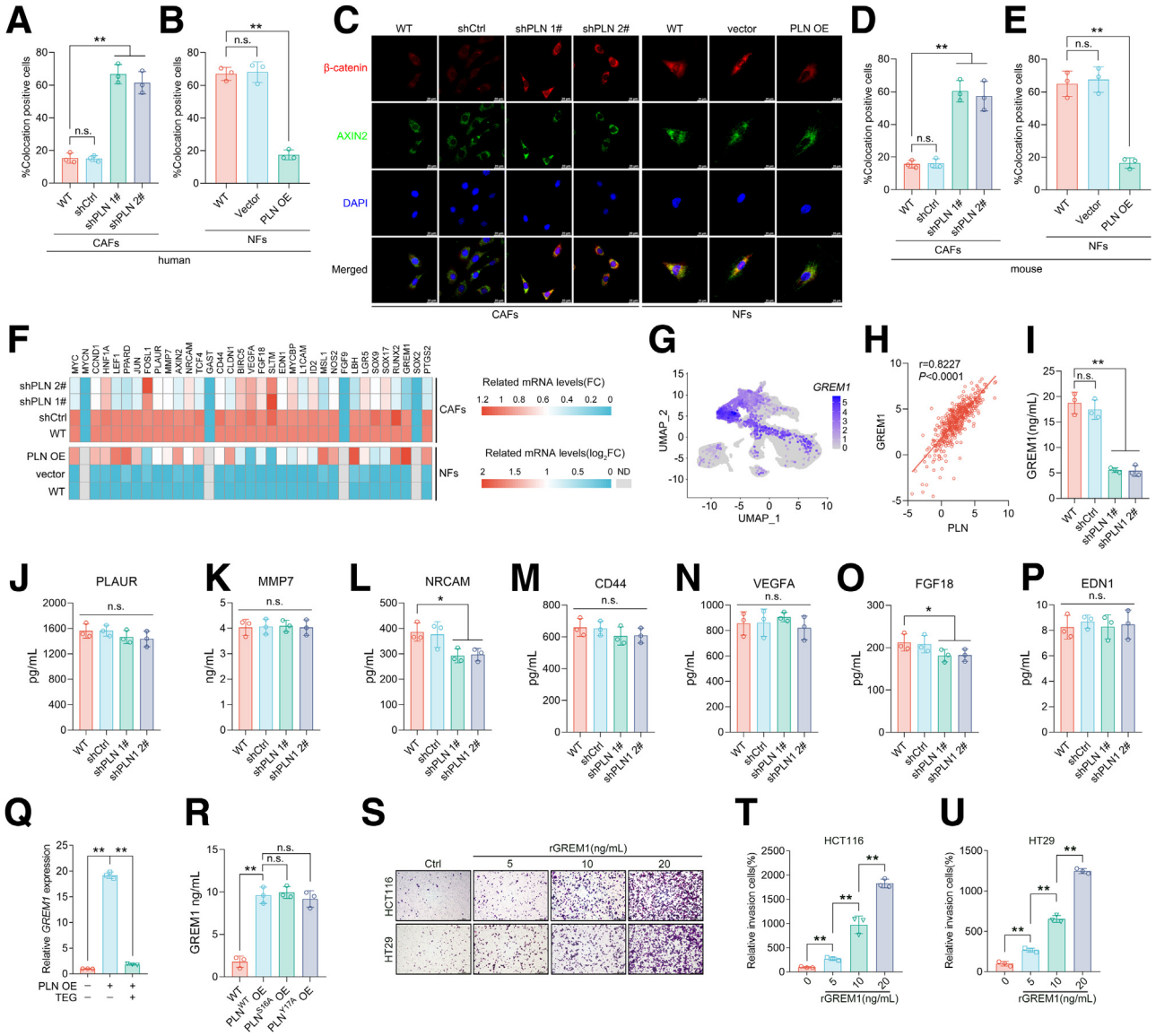

Figure 7. (*A–B*) quantification of immunofluorescence assay in Figure 6*P*. (*C–E*) representative images and colocation positive cells of immunofluorescence assay for β-catenin and AXIN2 in mouse CAFs transfected with shCtrl, shPLN-1#, or PLN-2#, or in NFs transfected with empty vector or PLN overexpression (OE). (*F*) heatmap for relative mRNA levels of Wnt/β-catenin target genes in wild-type (WT), shCtrl, shPLN 1#, and shPLN 2# transfected human sourced CAFs, or in WT, vector, and PLN OE transfected human-sourced NFs, as quantified by qPCR. FC, fold change. (*G*) UMAP plot of *GREM1* expression distribution in the scRNAseq data from CRC tumor tissues. (*H*) *GREM1* and *PLN* mRNA expression correlation analyzed by Spearman method in TCGA-COAD. (*I–P*) ELISA assay for GREM1, PLAUR, MMP7, NRCAM, CD44, VEGFA, FGF18, and EDN1 detection in human CAFs' CM. (*Q*) qPCR assay for *GREM1* mRNA detection in human CAFs (tegatrabetan [TEG], 10 μmol/L for 24 hours incubation). (*R*) GREM1 levels in supernatants of human CAFs with WT PLN OE, S16A mutated PLN OE, or Y17A mutated PLN OE. (*S–U*) representative photos and quantification of Transwell assay for HCT116 and HT29 cells after incubation with rGREM1 for 48 hours. All experiments have been repeated at least 3 times independently. *$P < .05$; **$P < .01$; n.s., no significant differences.

EMT and angiogenesis, which were the main features of the CMS4 subtype.

PLN-β-catenin-GREM1 Axis Promoted EMT and Angiogenesis Via BMP2 and VEGFR2 Signaling, Respectively

Secreted GREM1 was reported as a potent antagonist of bone morphogenetic protein (BMP).[14] BMPs, which are glycosylated extracellular matrix associated members of TGF-β, play crucial roles in negatively regulating cell differentiation. Previous studies have demonstrated that GREM1 specifically binds to BMP2, BMP4, and BMP7.[15] Based on the above knowledge, we first investigated whether PLN/β-catenin/GREM1 axis-induced EMT in CRC cells was mediated by BMPs. To test this hypothesis, BMP2/4/7 were overexpressed, or recombinant BMP2/4/7 protein were added in HCT116 and HT29 cells, and only BMP2

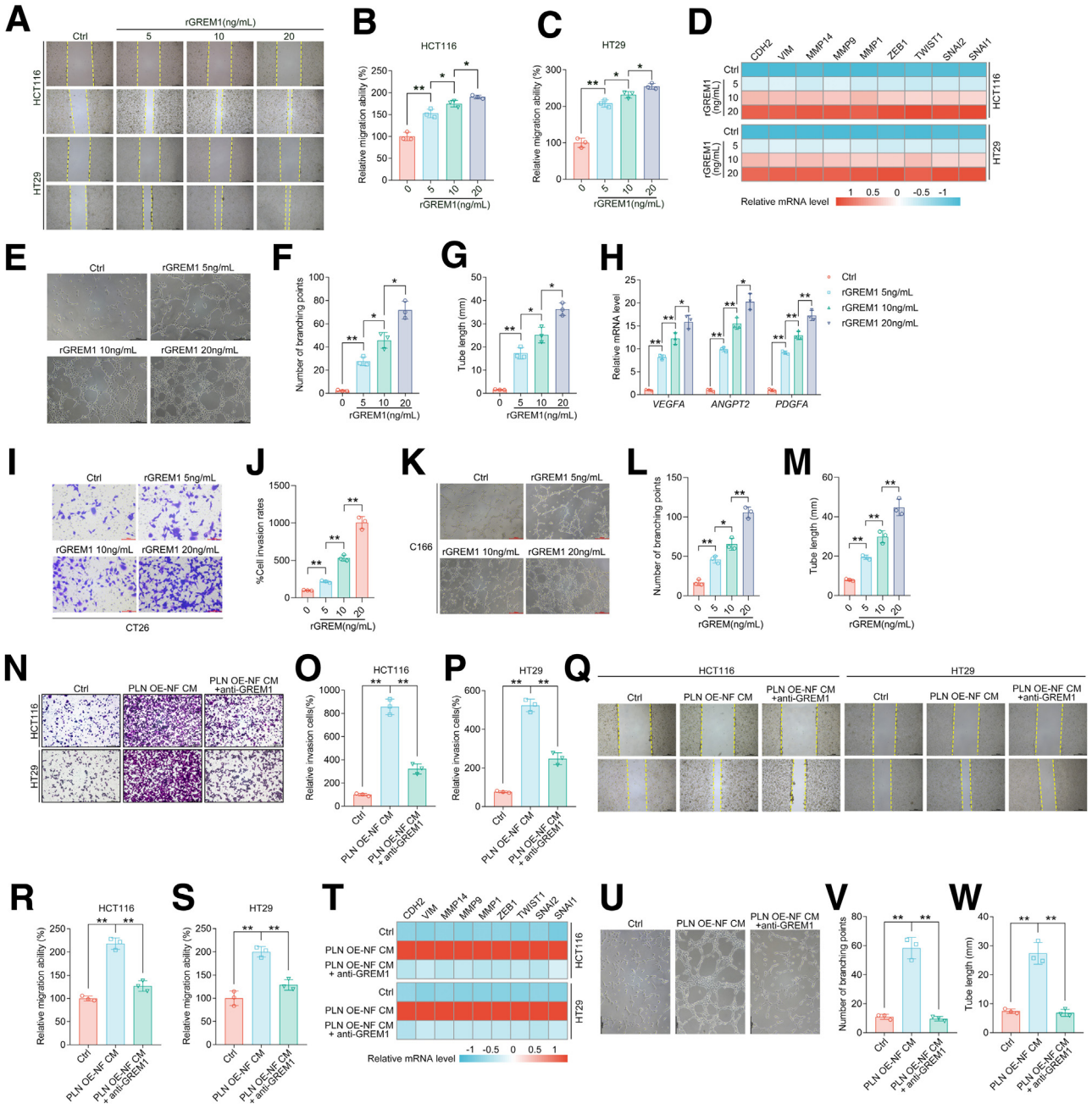

Figure 8. (*A–C*) Representative photos and quantification of wound-healing assay for HCT116 and HT29 cells after incubation with rGREM1 for 48 hours. (*D*) qPCR assay for EMT related genes of HCT116 and HT29 cells after incubation with rGREM1 for 48 hours. (*E–G*) representative photos and quantification of tube formation assay in HUVEC cells after incubation with/without rGREM1 for 48 hours. (*H*) qPCR assay for angiogenesis-related genes of HUVEC cells after incubation with/without rGREM1 for 48 hours. (*I–J*) representative images of Transwell assay and quantification for cell invasion rates in CT26 cells treated with recombinant GREM1 (5, 10, 20 ng/mL) for 48 hours. (*K–M*) Representative images of tube formation assay (*K*), quantification of branching points (*L*), and tube length (*M*) in C166 cells treated as described in (*I–J*). (*N–P*) Representative photos and quantification of Transwell assay for HCT116 and HT29 cells after incubation with PLN overexpressed NFs' CM (PLN OE-NF CM), and anti-GREM1 neutralizing antibody (Ginisortamab, 10 μg/mL) was administrated in 48 hours. (*Q–S*) Representative photos and quantification of wound healing assay for HCT116 and HT29 cells after incubation with PLN OE-NF CM, and anti-GREM1 neutralizing antibody (Ginisortamab, 10 μg/mL) was administrated in 48 hours. (*T*) qPCR assay for EMT related genes of HCT116 and HT29 cells after incubated with PLN OE-NF CM, and anti-GREM1 neutralizing antibody (Ginisortamab, 10 μg/mL) was administrated in 48 hours. (*U–W*) Representative photos and quantification of tube formation assay in HUVEC cells after incubation with PLN OE-NF CM, and anti-GREM1 neutralizing antibody (Ginisortamab, 10 μg/mL) was administrated in 48 hours. All experiments have been repeated at least 3 times independently. *$P < .05$; **$P < .01$.

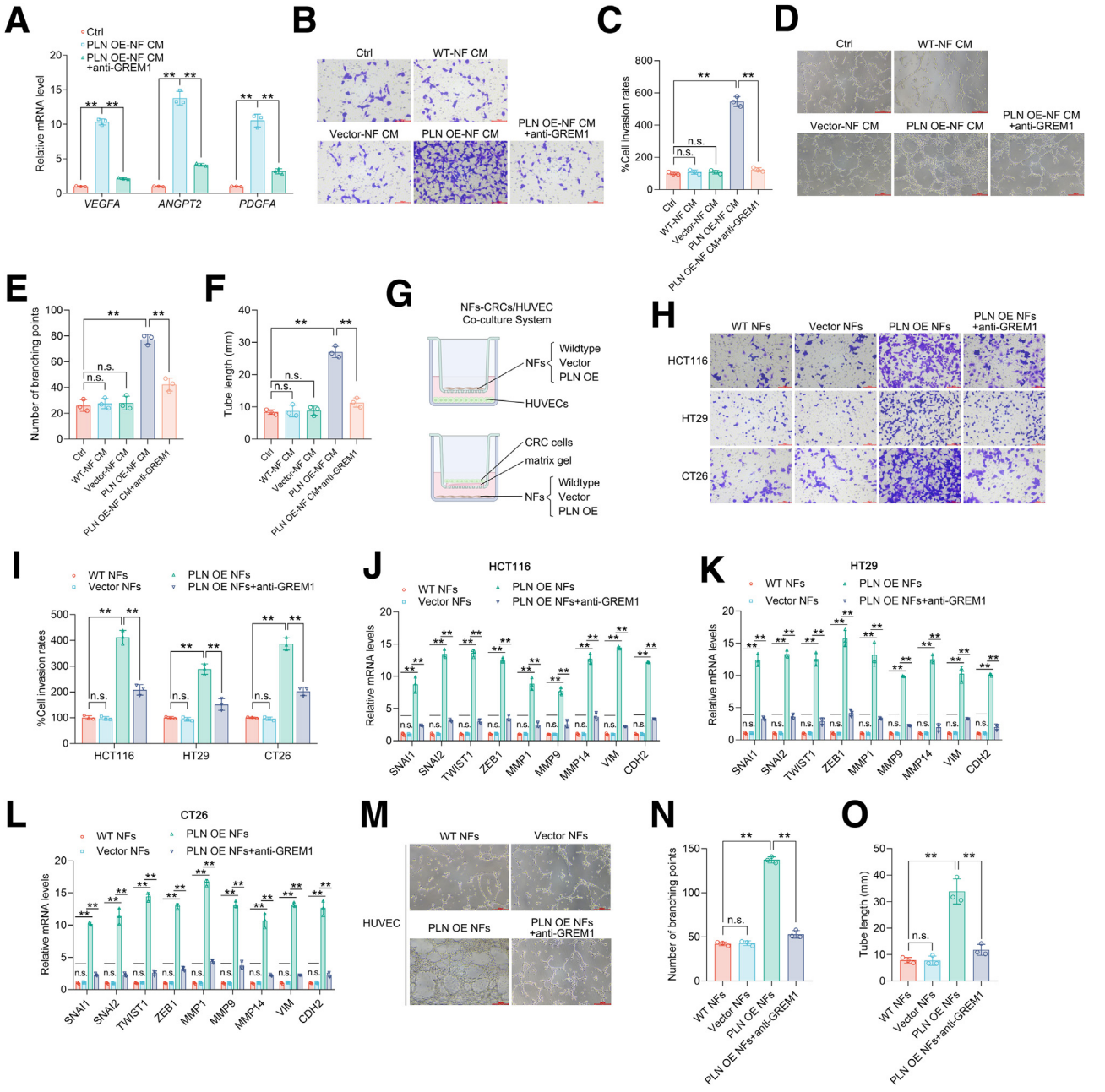

Figure 9. (*A*) qPCR assay for angiogenesis-related genes of HUVEC cells after incubated with PLN overexpressed NFs' CM (PLN OE-NF CM), and anti-GREM1 neutralizing antibody (Ginisortamab, 10 μg/mL) was administrated in 48 hours. (*B–C*) Representative images of Transwell assay and quantification for cell invasion rates in CT26 cells incubated with CM from mouse NFs transfected with empty vector, PLN OE and with/without anti-GREM1 neutralizing antibody (Ginisortamab, 10 μg/mL) for 48 hours. (*D–F*) Representative images of tube formation assay (*D*), quantification of branching points (*E*), and tube length (*F*) in C166 cells treated as described in (*B–C*). (*G*) Schematic diagram of NFs-CRC cell lines/HUVEC co-culture system based on Transwell plates. (*H–I*) Representative images of Transwell assay (*H*) and quantification of cell invasion rates (*I*) in HCT116, HT29, and CT26 incubated with CM from NFs transfected with empty vector, PLN OE and with/without anti-GREM1 neutralizing antibody (Ginisortamab, 10 μg/mL) for 48 hours. (*J–L*) qPCR analysis of EMT marker genes mRNA levels in HCT116, HT29, and CT26 cells treated as described in (*H–I*). (*M–O*) Representative images of tube formation assay (*M*), quantification of branching points (*N*), and tube length (*O*). All experiments have been repeated at least 3 times independently. $^{**}P < .01$. n.s., no significant differences.

overexpression or recombinant BMP2 (rBMP2) treatment significantly reversed EMT marker genes upregulation induced by CAF CM; in contrast, neither BMP4 nor BMP7 overexpression or their respective recombinant proteins treatments had any significant influences on CAF CM's such effects (Figure 10*B*). Furthermore, BMP2 overexpression or rBMP2 treatment in HCT116, HT29, and CT26 cells effectively reversed CAF CM-induced cell invasion and migration

(Figure 10*C–H*), indicating that CAF-derived PLN/*β*-catenin/GREM1 axis promoted CRC cell EMT by inhibiting BMP2 signaling.

We next investigated whether CAF CM-mediated angiogenesis also occurs via BMPs signaling inhibition. Intriguingly, neither BMP2/4/7 overexpression nor recombinant

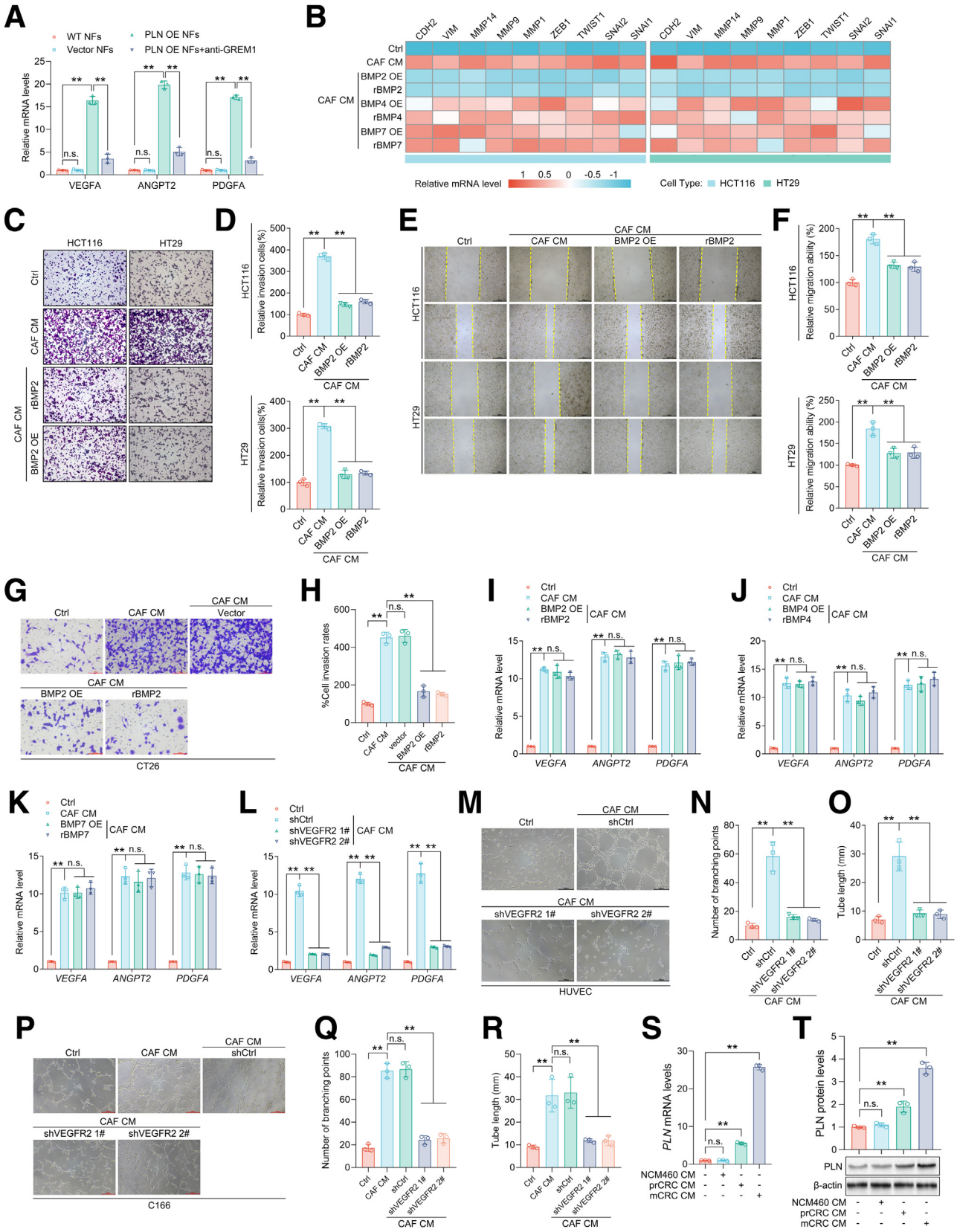

protein treatments in HUVEC cells significantly affected influences the upregulation of angiogenesis-related genes induced by CAF CM (Figure 10*I–K*). These results demonstrated that PLN/β-catenin/GREM1 axis promoted angiogenesis through a BMP-independent manner. Previous studies have identified GREM1 as an agonist of VEGF receptor-2 (VEGFR2), which was the primary mediator of VEGF-induced angiogenic signaling.[16] So we tried to verify whether PLN/βcatenin/GREM1 axis induced angiogenesis via VEGFR2 in context of CRC TME. The results showed that VEGFR2 knockdown significantly reversed CAF CM-induced upregulation of angiogenesis-related genes and mesh formation in both HUVEC and C166 cells (Figure 10*L–R*), which demonstrated that PLN/β-catenin/GREM1 axis promoted angiogenesis via VEGFR2 signaling.

CRC Cancer Cells Induced PLN Upregulation in NFs Via VTN/ITGB1 Signaling

We further investigated how PLN retained high levels in CAFs. Firstly, we found that CM from CRC cancer cells incubation significantly increased mRNA and protein levels of PLN in NFs, and metastatic CRC cancer cell (mCRC)-derived CM had more aggressive effects on PLN expression than primary CRC cancer cell (prCRC), whereas there were no significant changes on PLN expression during normal colorectal epithelial cell (NCM460) CM incubation, indicating that CRC cancer cells are responsible for PLN regulation in CAFs (Figure 10*S–T*). We then subclustered CAFs in CRC cancer scRNAseq data, which showed that PLN were mainly expressed in myofibroblastic CAFs (myCAFs, a subtype reported to strong induce tumor metastasis, and its enrichment in the TME is an important feature of CMS4 subtype CRC) (Figure 11*A*); and what's more, both prCRC and mCRC CMs incubation induced myCAFs; markers upregulation in NFs, indicating that CRC cancer cells can induce oriented conversion of fibroblasts phenotype (Figure 11*B*).

To understand how CRC cancer cells (especially mCRC) regulate PLN levels in CAFs, we carried out cell communication analysis between mCRC and myCAFs in the scRNAseq data, and the results showed that 91 ligand-receptor pairs had been predicated from mCRC to myCAFs (Figure 11*C–D*). We knocked down the top scored pairs via short hairpin RNA (shRNA), and found that only integrin subunit beta 1 (ITGB1) knockdown in NFs or vitronectin (VTN) knockdown in mCRC could block mCRC CM-induced PLN as well as myCAFs markers upregulation in NFs (Figure 11*E–P*), indicating that CRC cancer cells secrete VTN, which activates ITGB1 on fibroblasts to induce PLN expression and phenotype transformation towards myCAFs.

CAF-derived PLN Signaling Promoted CRC Metastasis

Given that our *in vitro* findings had demonstrated that CAF CM could induce EMT and angiogenesis in a PLN-dependent manner, we further investigated the roles of CAF-derived PLN in CRC metastasis using a CAF-CT26 spleen co-transplantation mouse model (Figure 12*A*). Co-transplantation of CT26 with mouse CAFs resulted in increased metastasis nodules and larger tumor volumes compared with CT26 transplantation alone; importantly, PLN knockdown in CAFs significantly attenuated co-transplantation and led pro-metastasis effects (Figure 12*B–D*). Immunohistochemical analysis revealed protein levels of EMT marker vimentin (VIM) and angiogenesis marker CD31 were significantly increased in metastasis tissues from CAF-CT26 co-transplantation group, whereas VIM and CD31 were not increased in 2 PLN knockdown groups when compared with CT26 transplantation group (Figure 12*E–F*). The above results indicated that CAF-derived PLN signaling promoted CRC metastasis and drove CMS4 subtype formation.

Discussion

As highlighted in the introduction section, CMS4 is the most aggressive subtype of CRC with a high frequency of occurrence (23%), which makes its molecular diagnosis and precision treatment an urgent need. In this study, we explored the role of CAF-derived paracrine PLN signaling in driving CMS4-like phenotype remodeling within the TME of CRC. Mechanistically, CAF-sourced PLN maintains a high

Figure 10. (***See previous page***). **(*A*) qPCR analysis of angiogenesis marker genes mRNA levels in HUVEC cells qPCR analysis of angiogenesis marker genes mRNA levels in HUVEC cells incubated with CM from NFs transfected with empty vector, PLN overexpression (OE) and with/without anti-GREM1 neutralizing antibody (Ginisortamab, 10 μg/mL) for 48 hours.** (*B*) qPCR assay for EMT-related genes of HCT116 and HT29 cells after BMP2, BMP4, BMP7 overexpressed or 20 ng/mL rBMP2, rBMP4, rBMP7 treatments with CAF CM incubation. (*C–D*) Representative photos and quantification of Transwell assay for HCT116 and HT29 cells after BMP2 overexpressed or 20 ng/mL rBMP2 treatment with CAF CM incubation. (*E–F*) Representative photos and quantification of wound healing assay for HCT116 and HT29 cells after BMP2 overexpressed or 20 ng/mL rBMP2 treatment with CAF CM incubation. (*G–H*) representative images of Transwell assay and quantification for cell invasion rates in empty vector or BMP2 OE transfected CT26, or wildtype CT26 treated with rBMP2 (20 ng/mL), all under incubation with mouse CAFs CM for 48 hours. (*I–K*) qPCR assay for angiogenesis-related genes of HUVEC cells after BMP2, BMP4, BMP7 overexpressed or 20 ng/mL rBMP2, rBMP4, rBMP7 treatments with CAF CM incubation. (*L–O*) qPCR assay for angiogenesis-related genes, as well as representative photos and quantification of tube formation assay in HUVEC cells after VEGFR2 knockdown with CAF CM incubation. (*P–R*) Representative images of tube formation assay (*P*), quantification of branching points (*Q*), and tube length (*R*) in C166 cells transfected with shCtrl, shVEGFR2 1#, or shVEGFR2 2# and incubated with mouse CAFs CM for 48 hours. (*S*) relative mRNA levels of *PLN* in human NFs after incubation with CM from NCM460 (normal colon epithelial cells)、primary CRC cancer cells (prCRC), and metastasis CRC cancer cells (mCRC) for 48 hours, as quantified by qPCR. (*T*) Representative Western blotting bands and quantification of PLN protein levels in NFs treated with CM from NCM460, prCRC, and mCRC. All experiments have been repeated at least 3 times independently. n.s., no significant differences; $^{**}P < .01$.

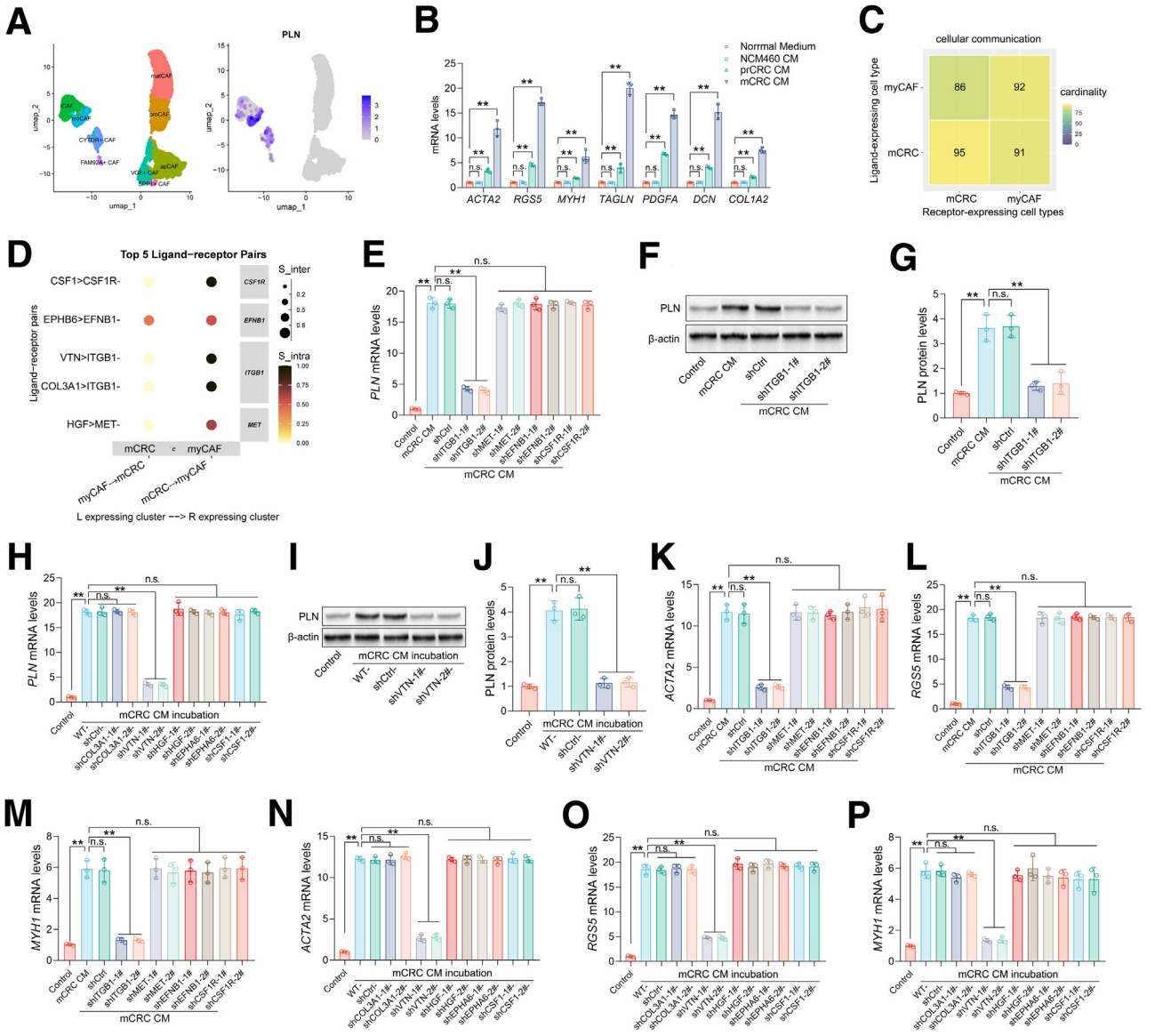

Figure 11. (*A*) Subclustering of CAFs and distribution of *PLN* expression in scRNAseq data from CRC tumor tissues (GSE225857, GSE231559, GSE178318, and GSE221575). (*B*) relative mRNA levels of myCAF maker genes in human NFs after incubation with CM from NCM460、prCRC, and mCRC for 48 hours, as quantified by qPCR. (*C–D*) Cell communication analysis between myCAF cluster and mCRC cluster in the scRNAseq data using the R package scSeqComm. (*E*) Relative mRNA levels of PLN in NFs transfected shITGB1, shMET, shEFBN1, or shCSF1R after incubation with mCRC CM for 48 hours, as quantified by qPCR. (*F–G*) Representative Western blotting bands (*F*) and quantification (*G*) of PLN protein levels in human NFs transfected with shCtrl, shITGB1-1# and shITGB1-2# after incubation with mCRC CM for 48 hours. (*H*) relative mRNA levels of *PLN* in NFs after incubation with CM from mCRC transfected shCOL3A1, shVTN, shHGF, shEPHA6, or shCSF1 for 48 hours, as quantified by qPCR. (*I–J*) Representative Western blotting bands (*I*) and quantification (*J*) of PLN protein levels in human NFs after incubation with CM from mCRC transfected with shCtrl, shVTN-1# and shVTN-2# for 48 hours. (*K–M*) Relative mRNA levels of myCAFs makers (*ACTA2, RGS5* and *MYH1*) in NFs transfected shITGB1, shMET, shEFBN1, or shCSF1R after incubation with mCRC CM for 48 hours, as quantified by qPCR. (*N–P*) Relative mRNA levels of myCAFs makers (*ACTA2, RGS5,* and *MYH1*) in NFs after incubation with CM from mCRC transfected shCOL3A1, shVTN, shHGF, shEPHA6, or shCSF1 for 48 hours, as quantified by qPCR. All experiments have been repeated at least 3 times independently. n.s., no significant differences; $^{**}P < .01$.

level, which upregulates β-catenin activity via competitively binding to AXIN2 and disrupting β-catenin degradation complex formation. CAF-derived Wnt/β-catenin signaling induces GREM1 expression and secretion into TME. Secreted GREM1 promotes cancer cell EMT and vascular endothelial cell angiogenesis through BMP2 and VEGFR2 signaling respectively, thereby driving CRC evolution into CMS4 subtype. In turn, CRC cancer cells sustain high PLN expression in CAFs and promote the transformation into a myCAFs phenotype via a VTN/ITGB1 paracrine signaling.

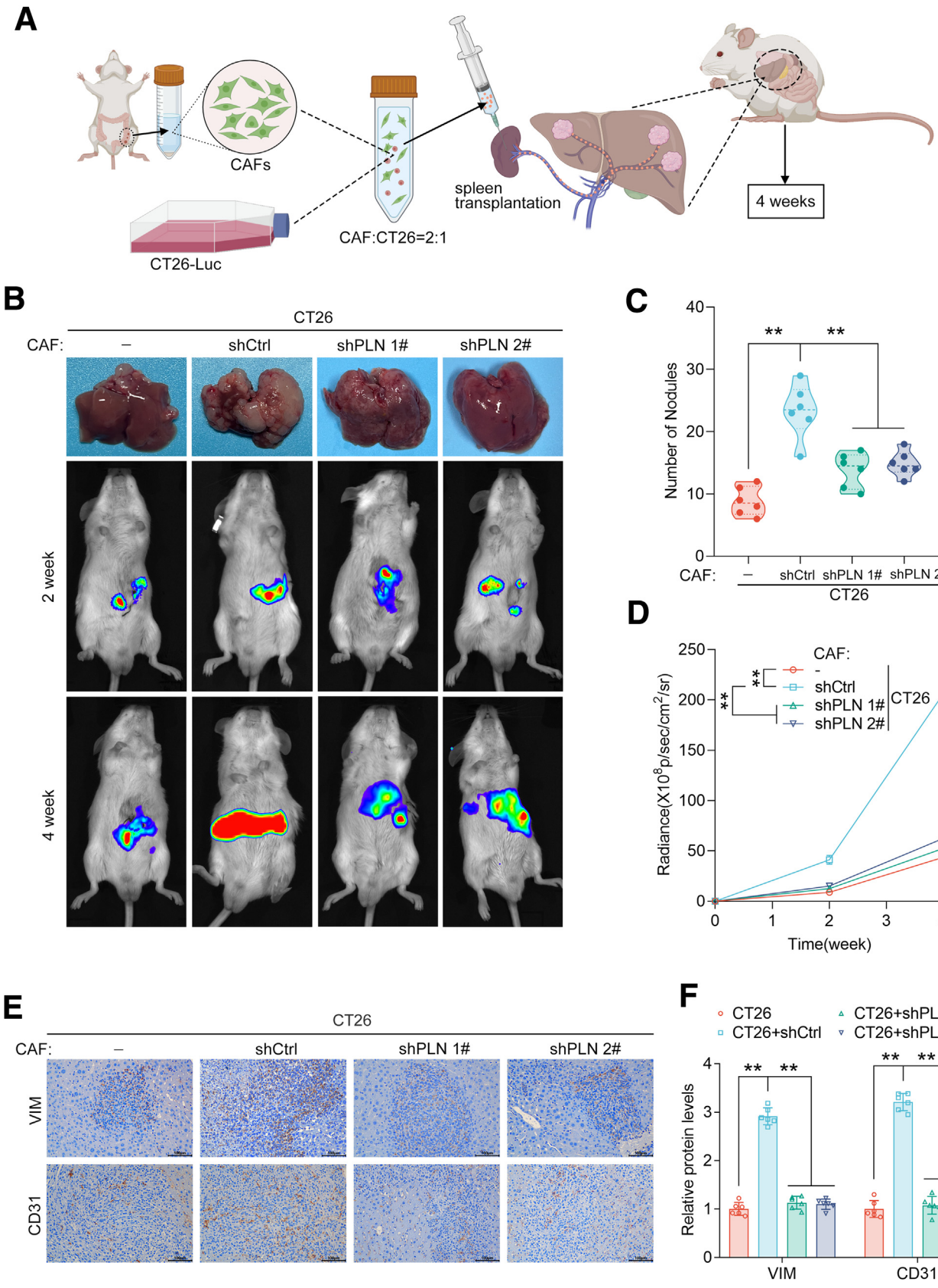

Figure 12. (*A*) Schematic diagram of the CAF-CT26 spleen co-transplantation mouse model (n = 6 in each group). (*B*) Representative photos of liver and *in vivo* bioluminescence imaging for each group. (*C–D*) Liver metastasis nodules and bioluminescence radiance of each group. (*E–F*) Representative photos and quantification of VIM and CD31 IHC assay. $^{**}P < .01$.

Our findings suggest that targeting PLN may serve as a promising strategy to develop precise diagnosis and treatment for CMS4 subtype CRC.

In recent decades, increasing research has emphasized the contributions of CAFs to cancer initiation, immune suppression, and treatment resistance.[17] For instance, CAFs have been shown to promote cancer cell proliferation by delivering exosomal microRNAs to cancer cells,[18] induce immune exclusion via chemokine secretion,[19] and contribute chemoresistance in lung and bladder cancers.[20] Here, we provide the first evidences for CAF-mediated CMS4-like phenotype remodeling, extending our understanding of CAFs' role in CRC progression. However, CAFs are a cluster of cells with high heterogeneity, which makes its regulation roles in TME multifaceted and even contradictory. In this study, we further identified myCAFs as the subtype responsible for PLN secretion in CRC TME, offering a more precise direction for PLN-based drug design.

The most interesting part of this study is the discovery of the cancer-promoting effects of CAF-derived PLN in CRC. PLN is commonly recognized as a key regulator of the cardiovascular system, but its physiologic and pathologic roles in the other systems remain largely unexplored. We demonstrated that PLN acts as an endogenous inhibitor of the β-catenin degradation complex to maintain high β-catenin activity. This effect is very similar to the well-known β-catenin degradation complex inhibitor, dishevelled (DVL), which disrupts the degradation complex by accumulating AXIN2 and GSK-3β at the cell membrane.[21] Although the Wnt/β-catenin signaling has long been implicated in cancer cell growth and invasion, its regulatory role in CAFs has not been paid enough attentions until recently.[22] Two previous studies have highlighted that CAFs derived Wnt/β-catenin signaling exhibits high activity and contributes to tumor growth, malignancy and angiogenesis.[23,24] However, the underlying cause of this elevated Wnt/β-catenin signaling activity in CAFs had remained unclear. Our findings provide a plausible explanation for this phenomenon, offering new insights into the role of PLN in CAF-mediated cancer progression.

We also found that *GREM1*, the Wnt/β-catenin signaling target gene, is upregulated and mediates the downstream effects of PLN/β-catenin axis, driving EMT in cancer cells and angiogenesis in vascular endothelial cells. GREM1, a high abundance protein detected in TME, has been demonstrated to be secreted by CAFs in various human cancers, including basal cell carcinoma, breast cancer, and CRC.[25] Consistent with our findings, previous studies have pointed out that CAFs-secreted GREM1 promotes cancer cell proliferation by blocking BMP signaling in CRC TME.[26] However, the specific BMP subtype blocked by GREM1 was not discussed yet, and we advanced this understanding by demonstrating that GREM1 specifically blocks BMP2 in the CRC TME. Additionally, we discovered that CAF-secreted GREM1 can induce angiogenesis with a BMP independent manner (the VEGFR2 signaling pathway), broadening the understanding of GREM1's roles in the context of CRC progression. Consistent with our findings, evidence had demonstrated that the regulation of BMP signaling on EMT is mediated by Notch and Smad intracellular pathways; additionally, GREM1/VEGFR2 induced angiogenesis via triggering intracellular signaling cascades similar with VEGF/VEGFR2, including PI3K/Akt and ERKs pathways.[27–30] In this study, we also investigated the causes of high PLN levels in CAFs, and found that PLN is distinctly high expressed in myCAFs subtype, and CRC cancer cell (especially metastasis cancer cell) is the driver for PLN high expression in CAFs and myCAFs phenotype transformation via a novel paracrine ITGB1-VTN signaling. Despite the critical role of CAFs in tumor progression being extensively studied over the past decade, few CAFs-targeted drugs have been designed for clinical cancer treatment, which is primarily attributed to the high heterogeneity of CAFs within a single TME as well as across cancer types. The generic strategies that targeted all types of CAFs without distinction may inadvertently challenge certain CAF populations with tumor suppressive effects (such as antigen-presenting CAFs), potentially compromising anti-tumor efficacy. To avoid this shortage, precisely targeting myCAF subtypes in TME via selective drug delivery system or special identification structure during PLN-targeted drug design should be taken into consideration.

However, there are some limitations to this study. We did not take deeper investigation into the mechanism by which the ITGB1-VTN paracrine signaling maintains high PLN levels in CAFs; and, we also did not further explore the reason why the phosphorylation status of PLN does not influence on its binding to AXIN2, despite evidence suggesting that PLN phosphorylation relieves the its interaction with ATP2A2.[11,12] Further investigations focusing on these limitations will favor better explanation of CAF-derived PLN signaling and its effects in CRC TME. In summary, this study uncovers a novel CAF-derived PLN/β-catenin/GREM1 signaling axis that plays a critical role in CMS4 subtype formation. PLN emerges as a promising target for molecular diagnosis and anti-metastasis therapy in CRC.

Materials and Methods

Chemicals and Regents

The chemicals and regents used in this study are listed in Table 1.

Clinical Samples

Clinical samples used in this study were provided by Nanjing First Hospital from 21 patients who were diagnosed with CRC between 2021 and 2023. This study was approved by the Ethics Committee of Nanjing First Hospital. All processes were conducted according to the principles in the Declaration of Helsinki, and the written patient informed consents of patients recruited in this study were deposited. Samples were separated into 2 parts; one part was fixed with 4% paraformaldehyde and the other was stored at −80 °C for further experiments.

Cell Culture

Human CAFs were isolated from CRC samples obtained from surgery, and NFs were isolated from the adjacent

Table 1. The Chemicals and Reagents Used in This Study

Reagent	Source	Identifier
Paraformaldehyde	Aladdin Biochemical	C104188
Crystal violet staining solution	Servicebio	G1014
Paraformaldehyde	Aladdin Biochemical	C104188
DNase I	Beyotime Biotechnology	D7073
Collagenase IV	Sigma-Aldrich	V900893
DMEM	Gibco	2230806
DMEM/F12	Gibco	21127030
Endothelial Growth Medium V2	Sigma-Aldrich	213-500
RPMI1640	Gibco	A1049101
F-12K	Gibco	21127030
McCoy's 5A	Gibco	16600082
Puromycin	Beyotime Biotechnology	ST551
Recombinant human GREM1	Proteintech	Ag12734
Recombinant human BMP2	Proteintech	HZ-1128
Recombinant human BMP4	Proteintech	HZ-1045
Recombinant human BMP7	Proteintech	HZ-1229
MG132	MedChemExpress	HY-13259
Cycloheximide	MedChemExpress	HY-12320
Ginisortamab	MedChemExpress	HY-P99643
Trizol reagent	Life Technologies	15596026
Human GAPDH Endogenous Reference Genes Primers	Sangon Biotech	B662104
Mouse GAPDH endogenous reference genes primers	Sangon Biotech	B662304
RIPA lysis buffer	Beyotime Biotechnology	P0013B
Acryl/Bis 30% solution	Sangon Biotech	B546017
1.5 mol/L Tris-HCl (pH 8.8)	Beyotime Biotechnology	ST789
1.0 mol/L Tris-HCl (pH6.8)	Beyotime Biotechnology	ST768
Sodium dodecyl sulfate, SDS	BioFroxx	3250GR500
Ammoniumpersulfate substitute, APS substitute	Beyotime Biotechnology	ST005
N,N,N',N'-Tetramethylethylenediamina, TEMED	Aladdin Biochemical	T105496
PVDF membrane	Merck Millipore	IPVH00010
Phenylmethanesulfonyl fluoride, PMSF	Beyotime Biotechnology	ST506
Isopropyl β-D-thiogalactoside, IPTG	Beyotime Biotechnology	ST098
Triton X-100	Beyotime Biotechnology	ST797
D-luciferin	Yeasen Biotechnology	40902ES03
Hematoxylin	Servicebio	G1004

tissues accordingly. Mouse CAFs were isolated from a CT26-based colon orthotopic transplantation mouse model. Briefly, tissues were digested by collagenase type IV (1 mg/mL) at 37 °C with agitation for 2 hours in Dulbecco's Modified Eagle Medium (DMEM)/F12 medium. The dissociated tissues were then filtered using 70-μm filters (Biosharp), followed by the separation of stromal cell-enriched supernatant to a new tube. The stromal fraction was collected by centrifuge at 250 g for 5 minutes. The isolated CAFs or NFs subsets were cultured in Endothelial Growth Medium V2 in a humidified incubator with 5% CO_2 at 37 °C.

HCT116, LOVO, HT29, SW480, and CT26 cell lines were purchased from the Cell Bank of Shanghai Institute of Biochemistry and Cell Biology. All cell lines were authenticated by short tandem repeat DNA test within 1 year (Shanghai Biowing Applied Biotechnology), and were free of *Mycoplasma* contamination. HCT116 and SW480 were cultured in DMEM medium; LOVO was cultured in F-12K medium; HT29 was cultured in McCoy's 5A medium; and CT26 was cultured in RPMI 1640 medium.

Animal Experiment

The construction of CAF-CT26 spleen co-transplantation mouse model was based on previous study.[31] Eight-week-old male BALB/c mice were assigned into 4 groups (CT26, CT26+CAF-shCtrl, CT26+CAF-shPLN 1#, and CT26+CAF-shPLN 2#), 6 mice for each group. CT26, or CT26: for CAFs, a 2:1 mixed cell suspension was injected into spleen of each group accordingly. Bioluminescence living imaging assays were carried out at the 14th and 28th day after cell transplantation. The experiment was ended on the 28th day, and liver

Table 2. shRNA Sequences Used in This Study

Species	Targets	Sequences
Human	PLN-1#	5′-GATCCCCTAACATCCAATGCAGGCAATTCAAGAGATTGCCTGCATTGGATGTTAGGTTTTTTG-3′
	PLN-2#	5′-GATCCGAAGAGCCTCAACCATTGAAATTCAAGAGATTTCAATGGTTGAGGCTCTTCTTTTTTG-3
	VEGFR2-1#	5′-GATCCGCGGCACGAAATATCCTCTTATTCAAGAGATAAGAGGATATTTCGTGCCGCTTTTTTG-3′
	VEGFR2-2#	5′-GATCCAGGCTAATACAACTCTTCAAATTCAAGAGATTTGAAGAGTTGTATTAGCCTTTTTTTG-3′
	ITGB1-1#	5′-GATCCGCCTTGCATTACTGCTGATATTTCAAGAGAATATCAGCAGTAATGCAAGGCTTTTTTG-3′
	ITGB1-2#	5′-GATCCGCCCTCCAGATGACATAGAAATTCAAGAGATTTCTATGTCATCTGGAGGGCTTTTTTG-3′
	MET-1#	5′-GATCCCAGAATGTCATTCTACATGAGTTCAAGAGACTCATGTAGAATGACATTCTGTTTTTTG-3′
	MET-2#	5′-GATCCGCTTACAAATAGCAACTACAATTCAAGAGATTGTAGTTGCTATTTGTAAGCTTTTTTG-3′
	EFBN1-1#	5′-GATCCCCAGAGCAGGAAATACGCTTTTTCAAGAGAAAAGCGTATTTCCTGCTCTGGTTTTTTG-3′
	EFBN1-2#	5′-GATCCAGCGACATCATCATTCCCTTATTCAAGAGATAAGGGAATGATGATGTCGCTTTTTTTG-3′
	CSF1R-1#	5′-GATCCGACTGACTTTATGCCTATGAATTCAAGAGATTCATAGGCATAAAGTCAGTCTTTTTTG-3′
	CSF1R-2#	5′-GATCCCTGCTGACTGTTGAGACCTTATTCAAGAGATAAGGTCTCAACAGTCAGCAGTTTTTTG-3′
	COL3A1-1#	5′-GATCCACACCGATGAGATTATGACTTTTCAAGAGAAAGTCATAATCTCATCGGTGTTTTTTTG-3′
	COL3A1-2#	5′-GATCCGCCAACCAGGAGAGAAGGGATTTCAAGAGAATCCCTTCTCTCCTGGTTGGCTTTTTTG-3′
	VTN-1#	5′-GATCCCCGAAATATCTCTGACGGCTTTTCAAGAGAAAGCCGTCAGAGATATTTCGGTTTTTTG-3′
	VTN-2#	5′-GATCCGAGGATGAGTACACGGTCTATTTCAAGAGAATAGACCGTGTACTCATCCTCTTTTTTG-3′
	HGF-1#	5′-GATCCCCCGTAATATCTTGTGCCAAATTCAAGAGATTTGGCACAAGATATTACGGGTTTTTTG-3′
	HGF-2#	5′-GATCCCAGACCAATGTGCTAATAGATTTCAAGAGAATCTATTAGCACATTGGTCTGTTTTTTG-3′
	EPHA6-1#	5′-GATCCCTGACCTCTTCCAAACTCTAATTCAAGAGATTAGAGTTTGGAAGAGGTCAGTTTTTTG-3′
	EPHA6-2#	5′-GATCCGCTCGGAATATACTGGTCAATTTCAAGAGAATTGACCAGTATATTCCGAGCTTTTTTG-3′
	CSF1-1#	5′-GATCCGACTGACTTTATGCCTATGAATTCAAGAGATTCATAGGCATAAAGTCAGTCTTTTTTG-3′
	CSF1-2#	5′-GATCCCTGCTGACTGTTGAGACCTTATTCAAGAGATAAGGTCTCAACAGTCAGCAGTTTTTTG-3′
Mouse	PLN-1#	5′-GATCCGCTGTGATAATCACTAAAGATTTCAAGAGAATCTTTAGTGATTATCACAGCTTTTTTG-3′
	PLN-2#	5′-GATCCGCTGATCTGCATCATTGTGATTTCAAGAGAATCACAATGATGCAGATCAGCTTTTTTG-3′
	VEGFR2-1#	5′-GATCCGCCGTCAAGATGTTGAAAGAATTCAAGAGATTCTTTCAACATCTTGACGGCTTTTTTG-3′
	VEGFR2-2#	5′-GATCCGCCCGTATGCTTGTAAAGAATTTCAAGAGAATTCTTTACAAGCATACGGGCTTTTTTG-3′

metastasis nodules were recorded. All procedures of the animal experiment were according to the protocols approved by the Animal Care and Use Committee of Nanjing First Hospital.

Plasmids and Lentivirus Transfection

Plasmid-encoded shRNA sequences against human PLN, VEGFR2, and mouse PLN genes were constructed by using lentivirus vector pLVX-shRNA2 (Cat# P0425, MiaolingBio; shRNA sequences are listed in Table 2). shRNA lentivirus particles were packaged in HEK293T cells by co-transfecting 2 auxiliary plasmids, PsPAX2 and pMD2.G. Target cells were then transfected with lentivirus and selected by puromycin (1 μg/mL). For PLN overexpression in CAFs, as well as BMP2, BMP4, and BMP7 overexpression in HCT116, HT29, or HUVEC, vector pEnCMV (Cat# P8196, MiaolingBio) was applied to load PLN, BMP2, BMP4, and BMP7 CDS sequences (NM_002667, NM_001200.4, NM_001202.6, and NM_001719.3). The shRNA interferences and overexpression efficiency had been verified via qPCR or Western blotting (Figures 13 and 14).

Transwell Assay

The method of Transwell assay was based on previous study.[31] Briefly, CRC cell lines (1×10^5 cells/well) were seeded in Matrigel coated chambers of Transwell plates. After indicated treatments, membranes of Transwell were fixed with 4% paraformaldehyde for 5 minutes, and washed by ddH_2O. The membranes were then stained for 15 minutes by crystal violet solution.

Wound-healing Assay

The method of wound-healing assay was based on previous study.[31] Briefly, CRC cell lines (1×10^6 cells/well) were seeded in 6-well plates. After 24 hours of incubation, cell attached surfaces were scratched straight lines with a 10-μL pipette tip and washed with phosphate-buffered saline (PBS) 3 times to clear the deciduous cells. Cells continued to incubate for another 24 or 48 hours with fetal bovine serum (FBS)-free medium. Cell scratch images were captured at 0, 24, and 48 hours after scratching, and migration rates were determined as: mean scratch area of 0 hour − mean scratch area of 24/48-hours)/mean scratch area of 0 hour × 100%.

Tube Formation Assay

Briefly, HUVEC cells were seeded in 96-well plates, which were coated with Matrigel with a density of 50,000 cells/well. Cells were cultured for 24 hours, and tube

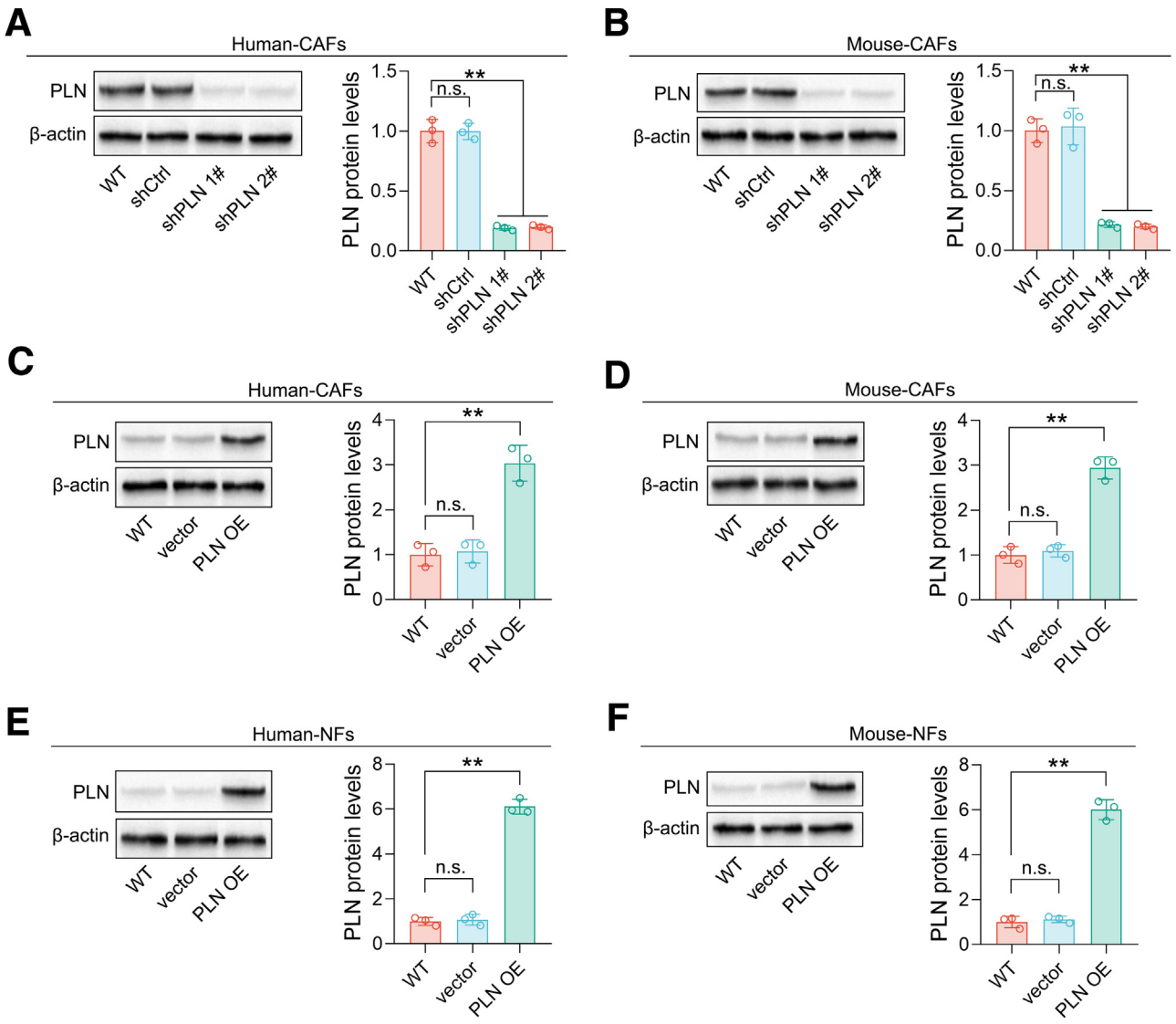

Figure 13. (*A–B*) Western blottings analysis of shRNA interferences efficiency targeting PLN in human and mouse CAFs. (*C–D*) Western blottings analysis of PLN overexpression efficiency in human and mouse CAFs. (*E–F*) Western blottings analysis of PLN overexpression efficiency in human and mouse NFs. All experiments have been repeated at least 3 times independently. n.s., no significant differences; $^{**}P < .01$.

formations were watched under an inverted microscopy. Image J software package was used for quantification analysis of tube formation.

Enzyme-linked Immunosorbent Assay

Briefly, CAFs' supernatants were collected at the end of experiments, and then a commercial enzyme-linked immunosorbent assay (ELISA) kit (Cat# E-EL-H1350, Elabscience) was used to detect GREM1 concentrations in CAFs' supernatants according to the instructions.

Real-time qPCR

The method of real-time qPCR was based on previous study.[31] Briefly, total RNAs from experimental samples (tissues and cells) were extracted by Trizol reagent, and quantified by a micro spectrophotometer. cDNAs were obtained from RNA templates by using EasyScript First-Strand cDNA Synthesis Super Mix Kit (Cat# AE301, Transgen). Real-time qPCR was conducted by using ChamQ SYBR qPCR Master Mix kits (Cat# Q421-02, Vazyme) in a 20-μL reaction system according to the instructions. Primers used in real-time qPCR were listed in Table 3. Relative mRNA expressions of detected genes were calculated by the $2^{-\Delta\Delta Ct}$ method with glyceraldehyde-3-phosphate dehydrogenase (GAPDH) as the internal control.

Western Blotting

The method of Western blotting was based on previous study.[31] Briefly, total protein of tissues and cells was extracted by RIPA buffer, and quantified by the BCA method. Protein samples were normalized and denaturation by incubated in boiled water for 5 minutes after adding loading

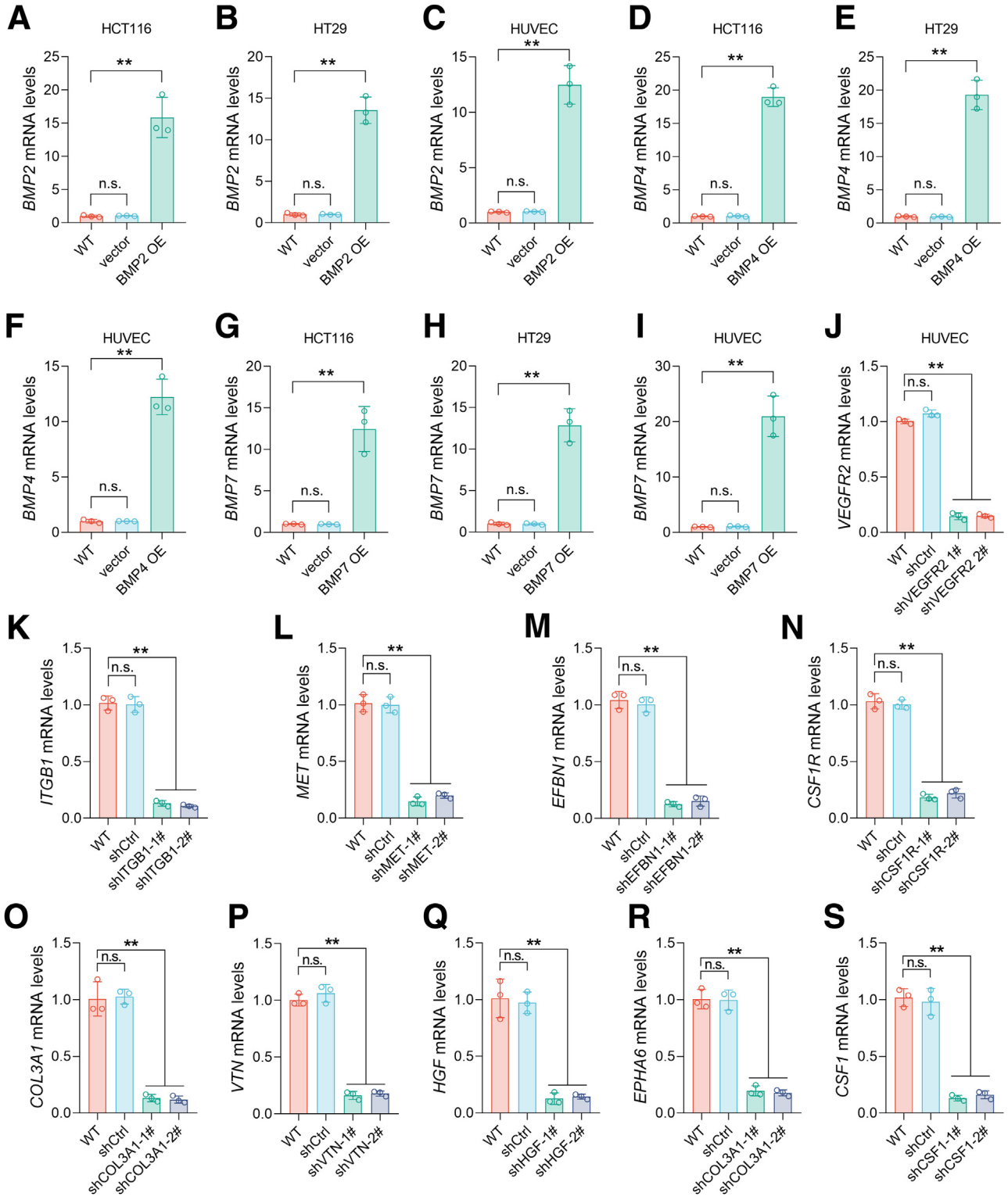

Figure 14. (*A–I*) qPCR analysis of efficiency BMP2, BMP4, and BMP7 overexpression in HCT116, HT29 and HUVEC cells. (*J*) qPCR analysis of shRNA interference efficiency targeting VEGFR2 in HUVEC cells. (*K–N*) qPCR analysis of shRNA interference efficiency targeting ITGB1, MET, EFBN1, and CSF1R in human NFs. (*O–S*) qPCR analysis of shRNA interference efficiency targeting COL3A1, VTN, HGF, EPHA6, and CSF1 in mCRC cells. All experiments have been repeated at least 3 times independently. n.s., no significant differences; $^{**}P < .01$.

Table 3. Primer Sequences for Targeted Genes Used in This Study

Species	Gene	Primer Sequences (5′-3′) Forward	Reverse
Human	*SFRP2*	ACGGCATCGAATACCAGAACA	CTCGTCTAGGTCATCGAGGCA
	MYH11	CGCCAAGAGACTCGTCTGG	TCTTTCCCAACCGTGACCTTC
	DES	TCGGCTCTAAGGGCTCCTC	CGTGGTCAGAAACTCCTGGTT
	CNN1	CGTGGTCAGAAACTCCTGGTT	GAGGCCGTCCATGAAGTTGTT
	ACTG2	GCGTGTAGCACCTGAAGAG	GAATGGCGACGTACATGGCA
	MGP	TCCGAGAACGCTCTAAGCCT	GCAAAGTCTGTAGTCATCACAGG
	THBS4	TGCTGCCAGTCCTGACAGA	GTTTAAGCGTCCCATCACAGTA
	PDGFA	GCAAGACCAGGACGGTCATTT	GGCACTTGACACTGCTCGT
	ANGPT2	AACTTTCGGAAGAGCATGGAC	CGAGTCATCGTATTCGAGCGG
	VEGFA	AGGGCAGAATCATCACGAAGT	AGGGTCTCGATTGGATGGCA
	SNAI1	TCGGAAGCCTAACTACAGCGA	AGATGAGCATTGGCAGCGAG
	SNAI2	CGAACTGGACACACATACAGTG	CTGAGGATCTCTGGTTGTGGT
	TWIST1	GTCCGCAGTCTTACGAGGAG	GCTTGAGGGTCTGAATCTTGCT
	ZEB1	GATGATGAATGCGAGTCAGATGC	ACAGCAGTGTCTTGTTGTTGT
	MMP1	AAAATTACACGCCAGATTTGCC	GGTGTGACATTACTCCAGAGTTG
	MMP9	TGTACCGCTATGGTTACACTCG	GGCAGGGACAGTTGCTTCT
	MMP14	GGCTACAGCAATATGGCTACC	GATGGCCGCTGAGAGTGAC
	VIM	GACGCCATCAACACCGAGTT	CTTTGTCGTTGGTTAGCTGGT
	CDH2	TCAGGCGTCTGTAGAGGCTT	ATGCACATCCTTCGATAAGACTG
	CTNNB1	AAAGCGGCTGTTAGTCACTGG	CGAGTCATTGCATACTGTCCAT
	GREM1	CGGAGCGCAAATACCTGAAG	GGTTGATGATGGTGCGACTGT
	MYC	GGCTCCTGGCAAAAGGTCA	CTGCGTAGTTGTGCTGATGT
	MYCN	ACCCGGACGAAGATGACTTCT	CAGCTCGTTCTCAAGCAGCAT
	CCND1	GCTGCGAAGTGGAAACCATC	CCTCCTTCTGCACACATTTGAA
	HNF1A	AACACCTCAACAAGGGCACTC	CCCCACTTGAAACGGTTCCT
	LEF1	AGAACACCCCGATGACGGA	GGCATCATTATGTACCCGGAAT
	PPARD	CAGGGCTGACTGCAAACGA	CTGCCACAATGTCTCGATGTC
	JUN	TCCAAGTGCCGAAAAAGGAAG	CGAGTTCTGAGCTTTCAAGGT
	FOSL1	CAGGCGGAGACTGACAAACTG	TCCTTCCGGGATTTTGCAGAT
	PLAUR	TGTAAGACCAACGGGGATTGC	AGCCAGTCCGATAGCTCAGG
	MMP7	GAGTGAGCTACAGTGGGAACA	CTATGACGCGGGAGTTTAACAT
	AXIN2	CAACACCAGGCGGAACGAA	GCCCAATAAGGAGTGTAAGGACT
	NRCAM	TCCAACCATCACCCAACAGTC	TGAGTCCCATTACGGGTCCAG
	TCF4	CAAGCACTGCCGACTACAATA	CCAGGCTGATTCATCCCACTG
	GAST	ATGCAGCGACTATGTGTGTATG	GCCCCTGTACCTAAGGGTG
	CD44	CTGCCGCTTTGCAGGTGTA	CATTGTGGGCAAGGTGCTATT
	CLDN1	CCTCCTGGGAGTGATAGCAAT	GGCAACTAAAATAGCCAGACCT
	BIRC5	AGGACCACCGCATCTCTACAT	AAGTCTGGCTCGTTCTCAGTG
	VEGFA	AGGGCAGAATCATCACGAAGT	AGGGTCTCGATTGGATGGCA
	FGF18	ACTTGCCTGTGTTTACACTTCC	GACCTGGATGTGTTTCCCACT
	SLTM	AGCGGCGGAACTTAGACATC	TTGCTCATGTGCCTCTTGATT
	EDN1	AGAGTGTGTCTACTTCTGCCA	CTTCCAAGTCCATACGGAACAA
	MYCBP	ATGGCCCATTACAAAGCCG	TTTCTGGAGTAGCAGCTCCTAA
	L1CAM	TGTCATCACGGAACAGTCTCC	CTGGCAAAGCAGCGGTAGAT
	ID2	AGTCCCGTGAGGTCCGTTAG	AGTCGTTCATGTTGTATAGCAGG
	MSL1	GCTTTCCGAGACATCCCAGAC	GGCTCCTCAATTCACGTTTACAA
	NOS2	TTCAGTATCACAACCTCAGCAAG	TGGACCTGCAAGTTAAAATCCC
	FGF9	ATGGCTCCCTTAGGTGAAGTT	CCCAGGTGGTCACTTAACAAAAC
	LBH	GCCCCGACTATCTGAGATCG	GCGGTCAAAATCTGACGGGT

Table 3. Continued

Species	Gene	Primer Sequences (5′-3′) Forward	Reverse
	LGR5	CTCCCAGGTCTGGTGTGTTG	GAGGTCTAGGTAGGAGGTGAAG
	SOX9	AGCGAACGCACATCAAGAC	CTGTAGGCGATCTGTTGGGG
	SOX17	GTGGACCGCACGGAATTTG	GGAGATTCACACCGGAGTCA
	RUNX2	TGGTTACTGTCATGGCGGGTA	TCTCAGATCGTTGAACCTTGCTA
	GREM1	CGGAGCGCAAATACCTGAAG	GGTTGATGATGGTGCGACTGT
	SOX2	GCCGAGTGGAAACTTTTGTCG	GGCAGCGTGTACTTATCCTTCT
	PTGS2	CTGGCGCTCAGCCATACAG	CGCACTTATACTGGTCAAATCCC
	ACTA2	GCGGACCATCATAGGTTCCTT	ACTGGCTTGTCTAACAGGATTCT
	RGS5	GACATGGCCCAGAAAAGAATCC	CACAAAGCGAGGCAGAGAATC
	MYH1	CCCTACAAGTGGTTGCCAGTG	CTTCCCTGCGCCAGATTCTC
	TAGLN	AGTGCAGTCCAAAATCGAGAAG	CTTGCTCAGAATCACGCCAT
	PDGFA	GCAAGACCAGGACGGTCATTT	GGCACTTGACACTGCTCGT
	DCN	ATGAAGGCCACTATCATCCTCC	GTCGCGGTCATCAGGAACTT
	COL1A2	GTTGCTGCTTGCAGTAACCTT	AGGGCCAAGTCCAACTCCTT
	ITGB1	CCTACTTCTGCACGATGTGATG	CCTTTGCTACGGTTGGTTACATT
	MET	AGCAATGGGGAGTGTAAAGAGG	CCCAGTCTTGTACTCAGCAAC
	EFNB1	TGGAGCCCGTATCCTGGAG	TTGGGGTCGAGAACTGTGCTA
	CSF1R	GGGAATCCCAGTGATAGAGCC	TTGGAAGGTAGCGTTGTTGGT
	COL3A1	GGAGCTGGCTACTTCTCGC	GGGAACATCCTCCTTCAACAG
	VTN	TGACCAAGAGTCATGCAAGGG	ACTCAGCCGTATAGTCTGTGC
	HGF	GCTATCGGGGTAAAGACCTACA	CGTAGCGTACCTCTGGATTGC
	EPHA6	CGCTGTTGGCGGATTCACT	CGCAAATGCCCATTCTGTAAGT
	CSF1	TGGCGAGCAGGAGTATCAC	AGGTCTCCATCTGACTGTCAAT
	BMP2	ACCCGCTGTCTTCTAGCGT	TTTCAGGCCGAACATGCTGAG
	BMP4	ATGATTCCTGGTAACCGAATGC	CCCCGTCTCAGGTATCAAACT
	BMP7	TCGGCACCCATGTTCATGC	GAGGAAATGGCTATCTTGCAGG
	VEGFR2	GGCCCAATAATCAGAGTGGCA	CCAGTGTCATTTCCGATCACTTT
Mouse	*Snai1*	CACACGCTGCCTTGTGTCT	GGTCAGCAAAAGCACGGTT
	Snai2	TGGTCAAGAAACATTTCAACGCC	GGTGAGGATCTCTGGTTTTGGTA
	Twist1	GGACAAGCTGAGCAAGATTCA	CGGAGAAGGCGTAGCTGAG
	Zeb1	ACCGCCGTCATTTATCCTGAG	CATCTGGTGTTCCGTTTTCATCA
	Mmp1a	AACTACATTTAGGGGAGAGGTGT	GCAGCGTCAAGTTTAACTGGAA
	Mmp9	GCAGAGGCATACTTGTACCG	TGATGTTATGATGGTCCCACTTG
	Mmp14	ACCCACACACAACGCTCAC	GCCTGTCACTTGTAAACCATAGA
	Vim	CGTCCACACGCACCTACAG	GGGGGATGAGGAATAGAGGCT
	Cdh2	AGGCTTCTGGTGAAATTGCAT	GTCCACCTTGAAATCTGCTGG
	Pln	AAAGTGCAATACCTCACTCGC	GGCATTTCAATAGTGGAGGCTC
	Ctnnb1	ATGGAGCCGGACAGAAAAGC	TGGGAGGTGTCAACATCTTCTT
	Grem1	GGGACCCTACTGCCAACAG	TTTGCACCAATCTCGCTTCAG
	Kdr	TTTGGCAAATACAACCCTTCAGA	GCTCCAGTATCATTTCCAACCA
	Pdgfa	GAGGAAGCCGAGATACCCC	TGCTGTGGATCTGACTTCGAG
	Angpt2	CCTCGACTACGACGACTCAGT	TCTGCACCACATTCTGTTGGA
	Vegfa	CTGCCGTCCGATTGAGACC	CCCCTCCTTGTACCACTGTC

buffer. Protein samples were then loaded onto SDS-PAGE gels and transferred to polyvinylidene fluoride (PVDF) membrane for immunoblotting analysis using the following primary antibodies: anti-PLN(Cat# ab219626, Abcam), anti-β-catenin (Cat# 51067-2-AP, Proteintech), anti-AXIN2(Cat# 20540-1-AP, Proteintech), anti-CK1 (Cat# 55192-1-AP, Proteintech), anti-GSK-3β (Cat# 82061-1-RR, Proteintech), anti-β-actin (Cat# 20536-1-AP, Proteintech), anti-His (Cat# 10001-0-AP, Proteintech), anti-GST (Cat# 10000-0-AP, Proteintech), and anti-ubiquitin (Cat# 10000-0-AP,

Proteintech). PVDF membranes were then incubated with corresponding secondary antibodies. Protein bands were visualized by enhanced chemiluminescence regents and quantified by Image J software package. β-actin was used as the internal control.

Co-IP

The method of Co-IP was based on previous study.[32] Briefly, CAF lysates were prepared by using RIPA buffer under the instruction, and the cell lysates were incubated with anti-PLN, or anti-β-catenin antibodies overnight (4 °C). The cell lysates were then incubated with protein A&G agarose beads for another 4 hours. The agarose beads were collected by centrifugation (1000 g, 5 minutes) and washed 5 times with PBS. Then the beads were boiled (5 minutes) and loaded onto SDS-PAGE gels and conducted with immunoblotting analysis as described at Western blotting section.

GST Pull-down Assay

GST-labeled AXIN2 and β-catenin, as well as His-labeled PLN and AXIN2, were expressed and purified by using pGEX-4T-3 prokaryotic expression system as previously described.[32] The GST-labeled fusion proteins were incubated with Glutathione Sepharose 4B for 2 hours at 4 °C, and then incubated with His-labeled fusion proteins for another 12 hours at 4 °C. The beads were collected by centrifugation (1000 g, 5 minutes) and washed 5 times with PBS. Then the beads were boiled (5 minutes) and loaded onto SDS-PAGE gels and conducted with immunoblotting analysis as described in the Western blotting section.

Immunofluorescence and Immunohistochemistry Analysis

The method of immunofluorescence and immunohistochemistry analysis were based on previous study.[31] Tissue samples were fixed with 4% paraformaldehyde, and tissue slices were prepared at 5 μm. For immunofluorescence analysis, tissue slices were incubated with anti-PLN antibody (rabbit sourced) and anti-EpCAM/anti-FAP antibodies (mouse sourced) for 24 hours at 4 °C and incubated with Alexa Fluor 647 goat anti-rabbit and Alexa Fluor 488 goat anti-mouse IgG secondary antibodies for another 4 hours at room temperature. DAPI solution was used to stain cell nucleus. For immunohistochemistry analysis, tissue slices were incubated with anti-PLN, VIM, and CD31 antibodies for 24 hours at 4 °C, and then incubated with DAB for coloration. Slices were imaged by an inverted fluorescence microscopy and quantified by Image J software package.

Bioinformatic Analysis

The R package CMScaller was used to identified CMS subtypes and the different expression genes of TCGA-COAD and GSE106582 datasets. R packages survival and survminer were used to analyze and visualize CRC patients' survival profile of dataset GSE17536 and GSE17537. R packages Seurat, Harmony, and scSeqComm were used to integrate and analyze scRNA-seq datasets of CRC (GSE225857, GSE231559, GSE178318, and GSE221575). R package clusterProfiler was used to analyze and visualize gene function enrichment analysis (Gene Ontology [GO] and Kyoto Encyclopedia of Genes and Genomes [KEGG]). Protein docking analysis of AXIN2 (Q9Y2T1) and PLN (P26678) was performed via an online tool pyDockWEB (https://life.bsc.es/pid/pydockweb) and visualized by PyMOL software package.

Statistics

Data in this study were presented as mean ± standard deviation (SD). SPSS 20.0 software package was used for statistical analysis. For the 2-group data, the Student t-test was used to calculate the differences; 1-way analysis of variance (ANOVA) was used for calculating differences of data from more than 2 groups, and the least significant difference method was used for post hoc multiple comparisons. P values $< .05$ were regarded as statistically significant.

References

1. Siegel RL, Miller KD, Goding Sauer A, et al. Colorectal cancer statistics, 2020. CA Cancer J Clin 2020; 70:145–164.
2. Dekker E, Tanis PJ, Vleugels JLA, et al. Colorectal cancer. Lancet 2019;394:1467–1480.
3. Guinney J, Dienstmann R, Wang X, et al. The consensus molecular subtypes of colorectal cancer. Nat Med 2015; 21:1350–1356.
4. Fessler E, Medema JP. Colorectal cancer subtypes: developmental origin and microenvironmental regulation. Trends Cancer 2016;2:505–518.
5. Simmerman HK, Jones LR. Phospholamban: protein structure, mechanism of action, and role in cardiac function. Physiol Rev 1998;78:921–947.
6. De Genst E, Foo KS, Xiao Y, et al. Blocking phospholamban with VHH intrabodies enhances contractility and relaxation in heart failure. Nat Commun 2022;13:3018.
7. Klocke B, Britzolaki A, Saurine J, et al. A novel role for phospholamban in the thalamic reticular nucleus. Sci Rep 2024;14:6376.
8. Ahmad Zawawi SS, Musa M. Dynamic co-evolution of cancer cells and cancer-associated fibroblasts: role in right- and left-sided colon cancer progression and its clinical relevance. Biology (Basel) 2022;11:1014.
9. Yoshida GJ. Regulation of heterogeneous cancer-associated fibroblasts: the molecular pathology of activated signaling pathways. J Exp Clin Cancer Res 2020; 39:112.
10. Gorski PA, Ceholski DK, Young HS. Structure-function relationship of the SERCA pump and its regulation by phospholamban and sarcolipin. Adv Exp Med Biol 2017; 981:77–119.
11. Bovo E, Jamrozik T, Kahn D, et al. Phosphorylation of phospholamban promotes SERCA2a activation by dwarf open reading frame (DWORF). Cell Calcium 2024;121: 102910.

12. Roof SR, Shannon TR, Janssen PML, Ziolo MT. Effects of increased systolic Ca2+ and phospholamban phosphorylation during β-adrenergic stimulation on Ca2+ transient kinetics in cardiac myocytes. Am J Physiol Heart Circ Physiol 2011;301:H1570–H1578.
13. Gorski PA, Ceholski DK, Young HS. Structure-function relationship of the SERCA pump and its regulation by phospholamban and sarcolipin. In: Krebs J, ed. Membrane Dynamics and Calcium Signaling. Springer International Publishing, 2017:77–119.
14. Kosinski C, Li VS, Chan AS, et al. Gene expression patterns of human colon tops and basal crypts and BMP antagonists as intestinal stem cell niche factors. Proc Natl Acad Sci U S A 2007;104:15418–15423.
15. Church RH, Krishnakumar A, Urbanek A, et al. Gremlin1 preferentially binds to bone morphogenetic protein-2 (BMP-2) and BMP-4 over BMP-7. Biochem J 2015;466:55–68.
16. Mitola S, Ravelli C, Moroni E, et al. Gremlin is a novel agonist of the major proangiogenic receptor VEGFR2. Blood 2010;116:3677–3680.
17. Biffi G, Tuveson DA. Diversity and biology of cancer-associated fibroblasts. Physiol Rev 2021;101:147–176.
18. Chen B, Sang Y, Song X, et al. Exosomal miR-500a-5p derived from cancer-associated fibroblasts promotes breast cancer cell proliferation and metastasis through targeting USP28. Theranostics 2021;11:3932–3947.
19. Costa A, Kieffer Y, Scholer-Dahirel A, et al. Fibroblast heterogeneity and immunosuppressive environment in human breast cancer. Cancer Cell 2018;33:463–479.e10.
20. Shi L, Zhu W, Huang Y, et al. Cancer-associated fibroblast-derived exosomal microRNA-20a suppresses the PTEN/PI3K-AKT pathway to promote the progression and chemoresistance of non-small cell lung cancer. Clin Transl Med 2022;12:e989.
21. Sharma M, Castro-Piedras I, Simmons GE, Pruitt K. Dishevelled: a masterful conductor of complex Wnt signals. Cell Signal 2018;47:52–64.
22. Powell SM, Zilz N, Beazer-Barclay Y, et al. APC mutations occur early during colorectal tumorigenesis. Nature 1992;359:235–237.
23. Mosa MH, Michels BE, Menche C, et al. A Wnt-induced phenotypic switch in cancer-associated fibroblasts inhibits EMT in colorectal cancer. Cancer Res 2020;80:5569–5582.
24. Unterleuthner D, Neuhold P, Schwarz K, et al. Cancer-associated fibroblast-derived WNT2 increases tumor angiogenesis in colon cancer. Angiogenesis 2020;23:159–177.
25. Sneddon JB, Zhen HH, Montgomery K, et al. Bone morphogenetic protein antagonist gremlin 1 is widely expressed by cancer-associated stromal cells and can promote tumor cell proliferation. Proc Natl Acad Sci U S A 2006;103:14842–14847.
26. Kobayashi H, Gieniec KA, Wright JA, et al. The balance of stromal BMP signaling mediated by GREM1 and ISLR drives colorectal carcinogenesis. Gastroenterology 2021;160:1224–1239.e30.
27. Jiang F, Qin Y, Yang Y, et al. BMP-4 and BMP-7 inhibit EMT in a model of anterior subcapsular cataract in part by regulating the Notch signaling pathway. Invest Ophthalmol Vis Sci 2023;64:12.
28. Shu DY, Ng K, Wishart TFL, et al. Contrasting roles for BMP-4 and ventromorphins (BMP agonists) in TGFβ-induced lens EMT. Exp Eye Res 2021;206:108546.
29. Claesson-Welsh L, Welsh M. VEGFA and tumour angiogenesis. J Intern Med 2013;273:114–127.
30. Liu Y, Li Y, Hou R, Shu Z. Knockdown GREM1 suppresses cell growth, angiogenesis, and epithelial-mesenchymal transition in colon cancer. J Cell Biochem 2019;120:5583–5596.
31. Li T, Wei L, Zhang X, et al. Serotonin receptor HTR2B facilitates colorectal cancer metastasis via CREB1-ZEB1 axis-mediated epithelial-mesenchymal transition. Mol Cancer Res 2024;22:538–554.
32. Li T, Fu B, Zhang X, et al. Overproduction of gastrointestinal 5-HT promotes colitis-associated colorectal cancer progression via enhancing NLRP3 inflammasome activation. Cancer Immunol Res 2021;9:1008–1023.

Received September 7, 2024. Accepted April 18, 2025.

Correspondence
Address correspondence to: Qianming Du, PhD, General Clinical Research Center, Nanjing First Hospital, Nanjing Medical University, Nanjing 210006, P.R. China. e-mail: duqianming@njmu.edu.cn; Chao Liu, PhD, Department of Pharmacy, Nanjing First Hospital, Nanjing Medical University, Nanjing 210029, P.R. China. e-mail: liuchaogermany@sina.cn; or Xu Zhang, PhD, Department of Pharmacy, Chengdu Integrated TCM & Western Medicine Hospital, Chengdu University of TCM, 18# Wanxiang East Road, Chengdu, 610041, P. R.China. e-mail: xuzhang1989@cdutcm.edu.cn.

CRediT Authorship Contributions
Tao Li, PhD (Data curation: Equal; Funding acquisition: Supporting; Investigation: Lead; Methodology: Lead; Visualization: Lead; Writing – original draft: Lead)
Yuxiang Fei (Data curation: Equal; Investigation: Equal; Project administration: Lead; Validation: Equal; Visualization: Equal; Writing – original draft: Equal)
Xu Sun (Formal analysis: Equal; Investigation: Equal; Methodology: Equal; Validation: Equal; Visualization: Equal; Writing – original draft: Equal)
Jun Zhu (Investigation: Supporting; Resources: Supporting; Software: Supporting)
Xin Fang (Data curation: Supporting; Investigation: Supporting)
Fanjun Meng (Investigation: Supporting; Resources: Supporting)
Danyi Wang (Data curation: Supporting; Investigation: Supporting)
Xu Zhang (Conceptualization: Equal; Supervision: Equal)
Chao Liu (Conceptualization: Equal; Funding acquisition: Supporting; Supervision: Equal; Writing – review & editing: Equal)
Qianming Du, PhD (Conceptualization: Lead; Funding acquisition: Supporting; Supervision: Lead; Writing – review & editing: Supporting)

Conflicts of interest
The authors disclose no conflicts.

Funding
This study was supported by the National Natural Science Foundation of China (Nos. 82303498, 82172558, 82373112, 82273971, 82204394, 82274163, and 81803763), the Natural Science Foundation of Jiangsu (BK20231129), Hospital Pharmacy Foundation of Nanjing Pharmaceutical Association-Changzhou SiYao Pharmaceuticals (2022YX009 and 2022YX010), Nanjing Special Foundation for Health Science and Technology Development Project (YKK22122), and Key Projects of Health Technology Development Program of Luhe District (LHZD2024004).